Transition strengths and new band structures in odd-odd ^{78}Rb

R. A. Kaye, J. Döring, J. W. Holcomb,* G. D. Johns, T. D. Johnson,† M. A. Riley, G. N. Sylvan, P. C. Womble,‡ V. A. Wood, and S. L. Tabor
Department of Physics, Florida State University, Tallahassee, Florida 32306

J. X. Saladin
Department of Physics and Astronomy, University of Pittsburgh, Pittsburgh, Pennsylvania 15260
(Received 8 May 1996)

High-spin states in ^{78}Rb were studied using the ^{54}Fe(^{28}Si,3pn) reaction at 120 MeV and the ^{58}Ni(^{23}Na,2pn) reaction at 65 and 70 MeV. Prompt and delayed γ-γ coincidences were measured using the Pitt-FSU detector array. Results from these experiments have led to new levels partly grouped into new bands, new spin-parity assignments, and a rearrangement of the low-lying portion of the level scheme. States were observed up to (19^+) and (15^-) in the lowest energy positive- and negative-parity bands. Spin assignments were based on both directional correlation of oriented nuclei ratios and angular distributions. For some low-lying levels parity assignments were supported by a measurement of the linear polarizations of γ rays. Lifetimes were determined using the Doppler-shift attenuation method and direct timing. A reversal of signature splitting was observed in the yrast band at the 10^+ state. Large alternations were seen in the $B(M1)$ strengths in the yrast band, while the $B(E2)$ values in the two most strongly populated bands show a considerable collective enhancement. [S0556-2813(96)02409-0]

PACS number(s): 21.10.Tg, 23.20.En, 23.20.Lv, 27.50.+e

I. INTRODUCTION

Nuclei in the mass 80 region provide a fruitful testing ground for the study of a variety of shape and structural characteristics, such as large quadrupole deformations, the interaction of unpaired nucleons, and the competition between single-particle and collective excitations. These effects are dependent on the number of unpaired nucleons and the properties of the quasiparticle (qp) orbitals which they occupy. High-spin yrast states are expected to be based on the occupation of the unique parity $g_{9/2}$ subshell since it provides the highest angular momentum at the lowest energy for both proton and neutron qp in this mass region.

Although the low-lying level structure of odd-odd nuclei is complex, well-developed rotational bands starting at about 0.5 MeV excitation energy have been observed in a number of odd-odd nuclei in the $A\approx 80$ region. Recent studies on odd-odd nuclei, including ^{74}Br [1,2], ^{76}Br [3,4], ^{78}Br [5], ^{76}Rb [6], ^{80}Rb [7,8], ^{80}Y [9], and ^{82}Y [10–14], have indicated a considerable similarity among their yrast-band structures. A reversal of signature splitting, which was predicted [15] to result from the competition between single-particle and collective degrees of freedom, has been observed at a spin of approximately $9\hbar$ in each of these nuclei. Large alternations in the intraband magnetic dipole transition strengths $B(M1)$ are commonly observed in odd-odd nuclei. Furthermore, there is a tendency for the kinematic moments of inertia to converge [16] to approximately the rigid rotor value.

Characteristics such as these have not yet been reported for odd-odd ^{78}Rb. Some high-spin information is available, but apparent conflicts exist. The present investigation was initiated to examine ^{78}Rb in detail to learn more about its high-spin decay structure and, in the process, strengthen the knowledge of odd-odd nuclei as a whole in this mass region.

Previous investigations [17–19] of ^{78}Rb had identified an isomeric state with a half-life $T_{1/2}=5.74$ min and the ground state with $T_{1/2}=17.66$ min. Definite spins of 0 for the 17.66 min ground state and $4\hbar$ for the 5.74 min isomer were assigned [20,21] in atomic beam measurements. The first band structure was identified [22] up to an excitation energy of 1104.6 keV above the bandhead. Later this decay scheme was extended [23] to a tentative $15\hbar$ state 4143 keV above the bandhead. Tentative parity assignments of $0^{(+)}$ and $4^{(-)}$ for the ground state and the isomeric state, respectively, were based on prior β^+-decay measurements [17]. Electromagnetic decays of the isomer which determined its position were recently reported in a laboratory progress report [24]. The most recent study [25] reached tentative spins of 20, 21, 24, and $27\hbar$ in each of the four major cascades. However, very little detailed information is available about ^{78}Rb from this study, and a fifth band given in the level scheme has been previously placed [26] in ^{79}Sr.

A major problem with the existing level schemes of ^{78}Rb is that most of the states have been tentatively assigned negative parity, but the yrast bands in nearby odd-odd nuclei have positive parity. This problem could be solved if the tentative negative-parity assignment to the $I=4$ isomer could be reversed, but that would introduce another problem: missing negative-parity states. A more basic problem is that the two strongest decay sequences built on the isomer are so closely connected that it is hard to see how they could have

*Present address: Lockheed Martin Information Systems, Mail Point 800, Orlando, FL 32825.
†Present address: Department of Physics, University of Notre Dame, Notre Dame, IN 46556.
‡Present address: Oak Ridge National Laboratory, Mail Stop 6388, Oak Ridge, TN 37830.

opposite parity, as the systematics imply. A ''missing'' $7\rightarrow5$ $E2$ transition in the yrast cascade is another indication of difficulties with the existing level schemes.

An important goal of the present work was to reexamine the low-lying level scheme of ^{78}Rb to resolve these issues. Weaker γ-γ coincidence relations and possible doublets were explored to build a more comprehensive level scheme complete with as many linking transitions as possible. A search was made for missing and isomeric transitions down to 10 keV using a low-energy photon spectrometer (LEPS). Spin changes were investigated by measuring both directional correlation of oriented nuclei (DCO) ratios and angular distributions. Parity changes were examined through measurements of γ-ray linear polarizations using a three-detector Compton polarimeter. Altogether, these investigations led to some rearrangements in the low-lying portion of the level scheme which effectively decouple the two strongest cascades and show that the structure of ^{78}Rb is consistent with that of its odd-odd neighbors.

Although the half-lives of the isomer and the ground state had been determined, mean lifetimes of states above the isomer had not been extracted. Thus, another goal of the current investigation was to measure the mean lifetimes of higher-lying states using the Doppler-shift attenuation method (DSAM). This required the use of a thick target for the fusion-evaporation reaction and was aided by the use of the Pitt-FSU Compton-suppressed detector array [27]. The lifetime of one long-lived state was also determined using direct timing. The determination of lifetimes then allowed for the calculation of transition strengths, transition quadrupole moments, quadrupole deformations, and a better picture of the degree of collectivity in ^{78}Rb.

II. EXPERIMENTAL PROCEDURE

High-spin states in ^{78}Rb were studied via the ^{54}Fe(^{28}Si,$3pn$) and ^{58}Ni(^{23}Na,$2pn$) fusion-evaporation reactions at the Florida State University Tandem-LINAC facility. The ^{54}Fe target was 14 mg/cm^2 thick and enriched to 95.6%, while the ^{58}Ni target was 19.44 mg/cm^2 thick and enriched to 99.89%. Both reactions were used to measure γ-γ coincidences, while angular distributions and linear polarizations of γ rays were measured using the latter reaction only.

Two separate γ-γ coincidence measurements were performed. One experiment measured prompt coincidences using the ^{54}Fe(^{28}Si,$3pn$) reaction at 120 MeV. This measurement utilized the Pitt-FSU detector array [27] consisting of nine Compton-suppressed high-purity Ge (HPGe) detectors, four of which were placed at 145° with respect to the beam axis, three at 90°, and two at 35°. About 2×10^8 coincidences were collected on 8 mm magnetic tape. The data were sorted [28] into a triangular matrix with a dispersion of 0.5 keV/channel and consisting of all possible detector pairs, another triangular matrix with a dispersion of 0.8 keV/channel and containing coincidences between only the 90° detectors, and a square matrix with a dispersion of 0.8 keV/channel with coincidence information between the 145° and 90° detectors. Background-subtracted gated spectra projected from the triangular matrices yielded the γ-ray energies and intensities quoted in this paper. A similar energy gating technique used on the square matrix yielded DCO ratios as well as the line-shape information necessary to deduce mean lifetimes of nuclear states using the DSAM.

Both prompt and delayed γ-γ coincidences were measured with the ^{58}Ni(^{23}Na,$2pn$) reaction at 70 MeV. The Pitt-FSU detector array consisting of 10 Compton-suppressed HPGe detectors and one LEPS with a low-energy threshold of about 10 keV collected the γ-ray events. Approximately 1.5×10^7 events were collected and sorted in a variety of ways. The triangular and square matrices explained above were constructed in the same manner, thus providing an independent analysis of this nucleus. A square matrix containing the coincidences of 35° and 145° detectors versus 90° detectors and a square matrix consisting of coincidences between 145° detectors and all other detectors were also sorted to improve the statistics of the DCO ratio and DSAM lifetime analyses, respectively. One analysis technique available in this experiment was the ability to measure lifetimes of long-lived states using delayed coincidences. A time-to-amplitude converter (TAC) was started by a LEPS event and stopped by a signal from any one of the other 9 HPGe detectors. In this way a square matrix was built which consisted of LEPS energies and time differences from the TAC. Gates set on the LEPS energy spectrum resulted in prompt and/or delayed time events which have been analyzed to determine nanosecond lifetimes in ^{78}Rb.

Spins were assigned based on both DCO ratios and angular distribution measurements. The DCO ratios were determined whenever possible according to

$$R_{\mathrm{DCO}}=\frac{I_\gamma(\text{at } 35°,\ 145°;\ \text{gated by } \gamma_G \text{ at } 90°)}{I_\gamma(\text{at } 90°;\ \text{gated by } \gamma_G \text{ at } 35°,\ 145°)}. \quad (1)$$

If the gate γ_G represents one or more stretched electric quadrupole ($E2$) transitions, then the DCO ratios for stretched $E2$ transitions as well as for pure $M1$ $\Delta I=0$ transitions are expected to be approximately unity, while $\Delta I=1$ transitions yield ratios of about 0.5 if the multipole mixing ratio is small [29]. It was not possible to measure DCO ratios reliably for some weak transitions using $E2$ gates. In these cases, gates on nearby $\Delta I=1$ or $\Delta I=0$ transitions were used. Gates on pure $\Delta I=1$ transitions result in DCO ratios of approximately 1.0 and 2.0 for $\Delta I=1$ and stretched $E2$ transitions, respectively. All obtainable DCO ratios, along with level energies and spins, and relative intensities are given in Table I.

The linear polarizations of some strong low-lying decays were measured using the ^{58}Ni(^{23}Na,$2pn$) reaction at 65 MeV. A three HPGe detector geometry was used to detect the γ rays. One unshielded detector was oriented perpendicular to the beam direction and acted as the scattering detector. The other two detectors, which operated in coincidence with the scattering detector, were Compton suppressed with BGO shields and were oriented to detect radiation scattered parallel and perpendicular to the reaction plane. The coincidence data were saved to 8 mm tape and the two energies of each event were summed off line if they met the Compton-scattering condition. In this way, two spectra were produced showing γ rays scattered either parallel or perpendicular to the reaction plane. The linear polarization can then be calculated from the parallel intensity $N_\parallel$ and the perpendicular intensity $N_\perp$ according to

TABLE I. Energies, initial and final spin states, relative intensities, and DCO ratios for observed transitions in ^{78}Rb.

E_{lev} (keV)[a]	E_γ (keV)[b]	I_i^π	I_f^π	I_γ[c]	I_γ[d]	R_{DCO}[c,e]	R_{DCO}[d,e]
Band 1							
270.1	155.2(1)	5^+	4^+	100[f]	100[f]	0.44(5)	0.40(2)
422.8	152.7(1)	6^+	5^+	79(2)	79(2)	0.43(5)	0.39(3)
	307.9(1)	6^+	4^+	22(1)	26(1)	1.06(8)	0.97(6)
667.3	244.5(1)	7^+	6^+	45(1)	42(1)	0.47(6)	0.40(5)
	397.2(3)	7^+	5^+	6(1)	6(1)	1.20(50)	0.84(26)
852.9	185.6(2)	8^+	7^+	29(1)	28(1)	0.45(6)	0.49(8)
	430.1(2)	8^+	6^+	51(2)	53(2)	1.04(7)	0.95(8)
1219.7	366.8(1)	9^+	8^+	30(1)	33(1)	0.45(8)	0.42(5)
	552.4(2)	9^+	7^+	7(1)	7(1)	0.90(19)	0.95(11)
1625.5	405.8(2)	10^+	9^+	6(1)	7(1)	0.40(9)	0.49(11)
	772.6(2)	10^+	8^+	32(3)	37(3)	0.99(13)	0.98(16)
2023.6	398.1(2)	11^+	10^+	13(2)	21(2)	0.30(10)	0.41(10)
	803.9(3)	11^+	9^+	15(2)	21(2)	0.84(16)	0.85(12)
2651.1	627.5(3)	12^+	11^+	1.6(6)	1.7(5)	0.41(28)	0.49(5)
	1025.6(6)	12^+	10^+	9(3)	11(3)	0.73(22)	1.11(12)
3042.0	390.9(3)	13^+	12^+	1.7(4)	4(1)	0.17(35)	0.26(7)
	1018.4(5)	13^+	11^+	11(3)	13(3)	1.20(21)	0.93(16)
3897	1246(2)	(14^+)	12^+	2(1)	4(2)		
4253.7	1211.7(8)	(15^+)	13^+	4(2)	9(3)		
5639	1385(1)	(17^+)	(15^+)	1.2(5)	5(2)		
7192	1553(2)	(19^+)	(17^+)	0.8(4)	2(1)		
Band 2							
398.9	128.8(2)	$4^{(+)}$	5^+	2.8(3)	2.0(2)	1.16(8)[g]	1.26(7)[g]
	284.0(2)	$4^{(+)}$	4^+	4.6(6)	3.6(5)		0.78(9)
688.9	266.1(4)	$5^{(+)}$	6^+	0.8(2)	0.9(2)		1.28(14)[g]
	290.0(3)	$5^{(+)}$	$4^{(+)}$	3.2(4)	2.8(4)	1.07(15)[g]	0.79(22)[g]
736.8	47.9(3)	$6^{(+)}$	$5^{(+)}$				
	313.8(3)	$6^{(+)}$	6^+	2.4(5)	1.7(3)	0.84(39)	0.80(27)
	337.9(3)	$6^{(+)}$	$4^{(+)}$	2.3(6)	1.6(3)	1.76(25)[g]	1.92(44)[g]
	466.7(3)	$6^{(+)}$	5^+	6(1)	4.8(7)	0.87(5)[g]	0.81(6)[g]
1114.6	261.7(3)	$7^{(+)}$	8^+	1.1(3)	0.7(2)	1.15(16)[g]	1.14(11)[g]
	377.8(2)	$7^{(+)}$	$6^{(+)}$	4.1(6)	3.0(3)	1.02(9)[g]	1.26(12)[g]
	447.3(3)	$7^{(+)}$	7^+	0.9(3)	0.6(2)	0.72(35)[g]	1.33(38)[g]
1350.7	236.1(2)	$8^{(+)}$	$7^{(+)}$	1.9(4)	1.1(2)	1.12(12)[g]	0.97(8)[g]
	613.9(3)	$8^{(+)}$	$6^{(+)}$	1.4(4)	1.0(3)		
	683.4(3)	$8^{(+)}$	7^+	5.2(8)	3.4(5)	0.66(7)[g]	0.64(8)[g]
1454.2	339.6(3)	(8^+)	$7^{(+)}$	1.3(3)	0.7(2)	0.63(16)[g]	0.93(20)[g]
	717.4(4)	(8^+)	$6^{(+)}$	0.8(2)	0.8(3)		
1744.8	394.1(2)	$9^{(+)}$	$8^{(+)}$	2.8(5)	3.6(5)	1.19(17)[g]	1.26(12)[g]
	891.9(4)	$9^{(+)}$	8^+	2.2(8)	2.2(7)	0.49(23)	0.65(18)
	1077.5(3)	$9^{(+)}$	7^+	3(1)	1.6(3)	2.15(39)[g]	2.25(39)[g]
Band 3							
263.8	148.9(3)	5^-	4^+	≈ 2	≈ 2		
	152.6(1)	5^-	4^-	≈ 65	≈ 64	0.40(4)	0.41(3)
488.8	218.7(4)	6^-	5^+	1.2(3)	1.0(3)	1.26(18)[g]	1.30(18)[g]
	225.0(1)	6^-	5^-	27(1)	28(1)	0.37(6)	0.44(6)
	377.6(1)	6^-	4^-	19(1)	19(1)	1.08(12)	1.00(3)
767.1	278.3(2)	7^-	6^-	14(1)	14(1)	0.37(4)	0.43(11)
	344.3(4)	7^-	6^+	0.7(3)	0.4(2)	0.90(31)[g]	1.30(28)[g]
	503.3(3)	7^-	5^-	25(1)	23(1)	1.10(17)	1.07(12)
1114.4	347.3(3)	8^-	7^-	7.2(9)	7.9(8)	0.38(9)	0.43(3)
	625.6(3)	8^-	6^-	19(1)	22(1)	1.07(15)	0.98(3)

TABLE I *(Continued).*

$E_{\rm lev}$ (keV)[a]	E_γ (keV)[b]	I_i^π	I_f^π	I_γ [c]	I_γ [d]	$R_{\rm DCO}$[c,e]	$R_{\rm DCO}$[d,e]
1474.3	359.9(3)	9^-	8^-	3.8(6)	6.6(9)	0.47(11)	0.44(4)
	707.2(2)	9^-	7^-	18(2)	21(2)	0.95(7)	1.07(17)
1941.6	467.3(3)	10^-	9^-	2.8(7)	4.7(1.2)	0.46(11)	0.40(5)
	827.2(2)	10^-	8^-	13(2)	14(2)	0.89(8)	1.03(15)
2369.2	427.6(3)	11^-	10^-	0.7(2)	2.3(6)		0.50(7)
	894.9(4)	11^-	9^-	7(2)	9(2)	1.00(18)	0.91(13)
2955.4	1013.8(6)	12^-	10^-	6(2)	8(2)	1.06(23)	0.97(19)
3452.8	1083.6(7)	(13^-)	11^-	5(2)	6(2)		
4151	1196(1)	(14^-)	12^-	1.5(7)	1.6(6)		
4731	1278(2)	(15^-)	(13^-)	1.7(8)	3(1)		
Band 4							
395.6	68.1(3)	$4^{(-)}$	$3^{(+)}$	0.4(2)	0.4(2)		
	131.8(2)	$4^{(-)}$	5^-	2.2(3)	1.8(5)	1.25(16)[g]	0.73(13)[g]
	284.4(2)	$4^{(-)}$	4^-	8(1)	7(2)	1.76(24)[g]	1.61(14)[g]
595.3	155.2(2)	$5^{(-)}$	4^-	2.6(3)	4.4(4)	1.04(12)[g]	0.72(8)[g]
	199.7(2)	$5^{(-)}$	$4^{(-)}$	4.1(3)	3.1(2)	0.96(27)[g]	0.94(14)[g]
	331.5(2)	$5^{(-)}$	5^-	4.8(4)	4.9(4)	1.93(34)[g]	1.94(28)[g]
	484.1(3)	$5^{(-)}$	4^-	0.9(3)	0.9(3)		
872.2	276.9(1)	$6^{(-)}$	$5^{(-)}$	4.6(4)	4.1(2)	0.59(10)	0.54(19)
	383.4(2)	$6^{(-)}$	6^-	3.0(3)	2.2(2)	0.84(14)	1.02(12)
	476.6(4)	$6^{(-)}$	$4^{(-)}$	0.9(2)	0.6(1)		
1165.8	293.6(1)	$7^{(-)}$	$6^{(-)}$	2.6(4)	2.9(4)	0.51(12)	0.58(7)
	398.7(4)	$7^{(-)}$	7^-	0.4(2)	0.2(1)		
	570.5(3)	$7^{(-)}$	$5^{(-)}$	1.4(4)	1.8(4)	2.03(36) [g]	2.08(42) [g]
1603.6	437.8(3)	$8^{(-)}$	$7^{(-)}$	0.8(2)	1.1(2)	1.06(22) [g]	1.08(12) [g]
	731.4(6)	$8^{(-)}$	$6^{(-)}$	0.7(3)	0.9(3)		
1984.5	380.9(4)	(9^-)	$8^{(-)}$	0.3(1)	0.4(2)		
	818.7(4)	(9^-)	$7^{(-)}$	1.2(4)	1.7(5)		
Band 5							
46.8	46.8(2)	1^-	0^+				
134.1	87.3(2)	2^-	1^-	16(1)	$\approx$16	1.05(10)[g]	0.87(7)[g]
274.4	140.3(2)	3^-	2^-	11(1)	12(1)	0.94(8)[g]	1.29(10)[g]
	227.6(3)	3^-	1^-	1.8(5)	1.6(5)		
440.1	112.6(3)	4^-	$3^{(+)}$	4.2(5)	3.5(4)	0.92(12)[g]	0.95(20)[g]
	165.7(2)	4^-	3^-	3.9(4)	5.0(4)	1.08(10)[g]	1.17(12)[g]
	306.0(3)	4^-	2^-	0.5(3)	0.5(3)		
663.5	223.4(3)	5^-	4^-	3.2(7)	3.1(7)	0.95(12)[g]	1.35(16)[g]
	389.1(4)	5^-	3^-	0.5(3)	0.6(3)		
	399.7(3)	5^-	5^-	4(1)	4(1)	2.00(65)[g]	1.83(33)[g]
949.3	285.8(4)	6^-	5^-	1.1(3)	2.1(5)	1.01(29)[g]	0.82(13)[g]
	509.2(5)	6^-	4^-	0.4(2)			
1239.8	290.5(3)	7^-	6^-	0.7(2)	1.1(3)	1.01(29)[g]	1.34(35)[g]
	576.3(5)	7^-	5^-	0.4(1)	0.7(2)		
1678.0	438.2(4)	(8^-)	7^-	0.4(2)			
	728.7(6)	(8^-)	6^-	1.3(5)	0.8(4)		
2043.6	365.6(4)	(9^-)	(8^-)	< 0.4	< 0.4		
	803.8(5)	(9^-)	7^-	0.5(2)	0.9(3)		
Band 6							
475.9	148.4(3)	4^-	$3^{(+)}$	1.0(3)	1.0(2)	1.00(32)[g]	
	201.5(3)	4^-	3^-	2.4(4)	2.5(4)	1.16(12)[g]	0.99(16)[g]
	341.8(4)	4^-	2^-	1.6(4)	1.9(4)	1.87(33)[g]	
699.5	223.6(3)	5^-	4^-	1.7(4)	0.6(2)	1.06(14)[g]	1.12(24)[g]
	425.1(3)	5^-	3^-	1.8(4)	0.6(3)	2.02(68)[g]	

TABLE I. *(Continued).*

E_{lev} (keV)[a]	E_γ (keV)[b]	I_i^π	I_f^π	I_γ[c]	I_γ[d]	R_{DCO}[c,e]	R_{DCO}[d,e]
1017.4	317.9(4)	(6^-)	5^-	0.6(2)	0.5(1)		
	528.6(5)	(6^-)	6^-	1.2(4)	1.9(5)		
	541.5(5)	(6^-)	4^-	1.1(4)	0.7(2)		
1357.7	340.3(4)	(7^-)	(6^-)	< 0.4			
	658.2(6)	(7^-)	5^-	1.4(5)	1.0(4)		
Bands 7, 8, 9							
103.2	103.2(2)	1^+	0^+	21(5)	17(4)	0.93(6)[g]	0.88(11)[g]
160.7	57.5(2)	2^+	1^+	5.4(8)	3.2(3)	0.90(7)[g]	
	160.7(3)	2^+	0^+	2.7(3)	3.0(2)		1.94(48)[g]
232.4	98.3(2)	$2^{(+)}$	2^-	1.0(3)	0.4(1)		
	112.7(2)	$2^{(+)}$	(3^+)	1.2(3)	0.4(1)		
	129.2(3)	$2^{(+)}$	1^+	10(1)	10(1)	1.06(8)[g]	1.01(10)[g]
289.9	186.7(3)			2.1(6)			
	243.1(3)			4(1)			
	289.9(3)			1.3(5)			
315.4	181.3(4)	(2^+)	2^-	0.8(2)	1.4(3)		
	212.2(3)	(2^+)	1^+	6(1)	5(1)		
327.5	95.1(3)	$3^{(+)}$	$2^{(+)}$	4.8(4)	4.4(4)	0.99(10)[g]	
	193.4(3)	$3^{(+)}$	2^-	0.4(2)	0.2(1)		
	207.8(3)	$3^{(+)}$	(3^+)	1.8(5)			
	216.3(3)	$3^{(+)}$	4^-	1.5(4)			
334.2	173.5(2)	$3^{(+)}$	2^+	2.6(3)	1.8(2)	1.26(22)[g]	
	214.5(3)	$3^{(+)}$	(3^+)	2.9(4)	2.1(6)	1.95(34)[g]	2.01(33)[g]
	223.0(4)	$3^{(+)}$	4^-	0.8(3)	0.5(2)	1.19(34)[g]	1.39(35)[g]
351.0	190.3(2)	3^+	2^+	5.5(6)	4.2(3)	1.11(8)[g]	0.99(14)[g]
	247.8(3)	3^+	1^+	< 0.4			
504.0	214.1(4)			2(1)			
528.8	177.8(2)	4^+	3^+	1.8(3)	1.1(2)	1.23(34)[g]	
	194.6(3)	4^+	$3^{(+)}$	0.7(2)	0.4(1)	0.51(12)[h]	0.51(11)[h]
	368.1(4)	4^+	2^+	1.5(4)	1.9(4)	1.95(23)[g]	2.13(50)[g]
538.3	187.3(2)	$4^{(+)}$	3^+	2.8(4)	1.3(2)	1.02(9)[g]	
	204.1(3)	$4^{(+)}$	$3^{(+)}$	2.2(4)	1.9(2)	0.51(9)[h]	0.55(10)[h]
785.9	247.6(5)	$5^{(+)}$	$4^{(+)}$	1.8(4)	1.1(2)	0.40(16)[h]	
	257.1(3)	$5^{(+)}$	4^+	1.3(3)	0.7(2)		
824.9	286.6(3)	(5^+)	$4^{(+)}$	< 0.6			
	296.1(4)	(5^+)	4^+	< 0.4			
	473.9(4)	(5^+)	3^+	0.4(2)	0.7(3)		
1080.9	295.0(4)	(6^+)	(5^+)	2.1(4)	1.4(3)		
	552.1(5)	(6^+)	4^+	0.6(3)	0.6(2)		

[a]Energy of the initial state.
[b]γ-ray energies determined from an average of both reactions.
[c]Determined from the ^{58}Ni(^{23}Na,$2pn$) reaction.
[d]Determined from the ^{54}Fe(^{28}Si,$3pn$) reaction.
[e]DCO ratios were determined using one or more stretched $E2$ transitions unless otherwise noted.
[f]Normalization.
[g]DCO ratio determined using a gate set on one or more $\Delta I = 1$ transitions.
[h]DCO ratio determined using a gate set on the $\Delta I = 0$, 214 keV transition.

$$P_{\text{expt}} = \frac{1}{Q(E)} \frac{a(E)N_\perp - N_\parallel}{a(E)N_\perp + N_\parallel}, \tag{2}$$

where $a(E)$ is a relative normalization and $Q(E)$ is the polarimeter sensitivity. The normalization was obtained by assuming a vanishing polarization for the isotropic lines of a ^{152}Eu source. The sensitivity was determined by inverting the above equation and utilizing known [30] polarizations of lines in ^{78}Kr. The results of the polarization measurement (P_{expt}), along with theoretical polarizations (P_{thy}), are given in Table II.

Angular distributions of γ rays were measured with a single Compton-suppressed HPGe detector positioned at angles of 0°, 15°, 30°, 45°, 60°, 75°, and 90° relative to the

TABLE II. Angular distribution coefficients, mixing ratios, and experimental ($P_{\rm expt}$) and theoretical ($P_{\rm thy}$) linear polarizations determined for transitions in ^{78}Rb using the ^{58}Ni(^{23}Na,$2pn$) reaction.

E_γ (keV)	I_i^π	I_f^π	a_2	a_4	δ	$P_{\rm expt}$	$P_{\rm thy}$
87.3	2^-	1^-	−0.06(5)	−0.09(5)			
155.2	5^+	4^+	−0.31(4)	−0.04(4)	0.11(5)		
185.6	8^+	7^+	−0.31(4)	−0.08(4)	0.07(3)		
190.3	3^+	2^+	−0.30(6)	−0.01(7)	0.30(20)		
199.7	$5^{(-)}$	$4^{(-)}$	−0.27(5)	0.06(5)	0.03(5)		
214.5	$3^{(+)}$	(3^+)	0.22(8)	−0.02(10)			
225.0	6^-	5^-	−0.41(4)	−0.08(5)	0.38(11)	−0.29(11)	−0.07(5)
244.5	7^+	6^+	−0.29(4)	−0.09(5)	0.07(5)	−0.06(9)	−0.28(9)
278.3	7^-	6^-	−0.17(5)	0.01(5)			
284.4	$4^{(-)}$	4^-	0.23(4)	−0.09(6)			
293.6	$7^{(-)}$	$6^{(-)}$	−0.14(6)	0.03(7)			
307.9	6^+	4^+	0.41(5)	−0.11(7)	$E2$	1.10(12)	0.72(13)
331.5	$5^{(-)}$	5^-	0.26(8)	−0.06(8)			
347.3	8^-	7^-	−0.44(6)	0.01(6)	0.16(7)		
359.9	9^-	8^-	−0.48(9)	−0.07(9)	0.23(7)		
366.8	9^+	8^+	−0.40(6)	−0.09(6)	0.12(5)	−0.11(8)	−0.25(8)
377.6	6^-	4^-	0.25(6)	−0.10(8)	$E2$	0.40(8)	0.37(13)
383.4	$6^{(-)}$	6^-	0.46(9)	−0.35(10)			
405.8	10^+	9^+	−0.39(5)	0.06(6)	0.07(5)	−0.35(15)	−0.24(11)
430.1	8^+	6^+	0.48(4)	−0.21(7)	$E2$		
503.3	7^-	5^-	0.41(4)	−0.15(6)	$E2$		
552.4	9^+	7^+	0.34(6)	−0.08(8)	$E2$		
570.5	$7^{(-)}$	$5^{(-)}$	0.40(7)	−0.01(9)	$E2$		
625.6	8^-	6^-	0.36(5)	−0.04(7)	$E2$		
683.4	$8^{(+)}$	7^+	−0.38(9)	0.03(10)	0.07(11)		
707.2	9^-	7^-	0.50(6)	−0.02(8)	$E2$		
772.6	10^+	8^+	0.37(6)	−0.02(7)	$E2$		
803.9	11^+	9^+	0.17(6)	0.02(7)	$E2$		
827.2	10^-	8^-	0.27(7)	0.04(9)	$E2$		
894.9	11^-	9^-	0.48(9)	0.04(12)	$E2$		

beam axis. The peak areas were fitted and normalized to the intensities of the $6^+ \rightarrow 4^+$ 858 keV $E2$ line in ^{78}Kr [30]. A least-squares fit of the normalized intensities was then performed to a series of Legendre polynomials. All obtainable angular distribution coefficients and mixing ratios measured for ^{78}Rb are given in Table II. The signs of the a_2 coefficients agree with those given in Ref. [23]. A confirmation could not be made for the 1018 keV transition, which was too weak to permit a reliable measurement.

Theoretical angular distributions were calculated for each transition using a computer code which performs the necessary angular momentum algebra for particular initial and final spins of the decay and assuming a Gaussian distribution of magnetic substates. The width of the magnetic substate distribution σ was taken to be 2, although it has been shown [31] that the theoretical angular distributions are rather insensitive to values of σ between 0.5 and 2. By varying the mixing ratio δ over the range $\arctan(\delta) = -90°$ to 90°, curves of χ^2 were generated from a comparison of the theoretical angular distributions with the experimental data.

III. THE LEVEL SCHEME

The level scheme as deduced by coincidence measurements is shown in Figs. 1 and 2. The decay of the 4^- isomer [24], although not observed in this study, is included in Fig. 2 for completeness.

A. The 4^- isomer and its decay to the ground state

It was first suggested [22] that the high-spin sequences decay to the isomer, which is known [17–19] to have a half-life of $T_{1/2} = 5.74$ min. This hypothesis was further justified by an analysis [23] which demonstrated that the two strongest transitions in ^{78}Kr following the β^+ decay of ^{78}Rb produced in a heavy-ion reaction are consistent with the expected decay of a single activity with a half-life of 5.74 min. The current study has directly confirmed these findings with the discovery of linking transitions between the existing decay structure and the ground state (see Sec. III D).

The excitation energy of the isomer was previously [22,23] given as ''x,'' a number slightly larger than 103 keV, a known [17–19] transition associated with the isomer. A more recent study [24] has determined the isomeric decay scheme and assigned an excitation energy of 111.2 keV for the isomer, consistent with the new linking transitions mentioned above. They observed a highly converted 8.6 keV ($E3$) transition above the known 103.0 keV transition to the ground state. The 103 keV line has been assigned a multipo-

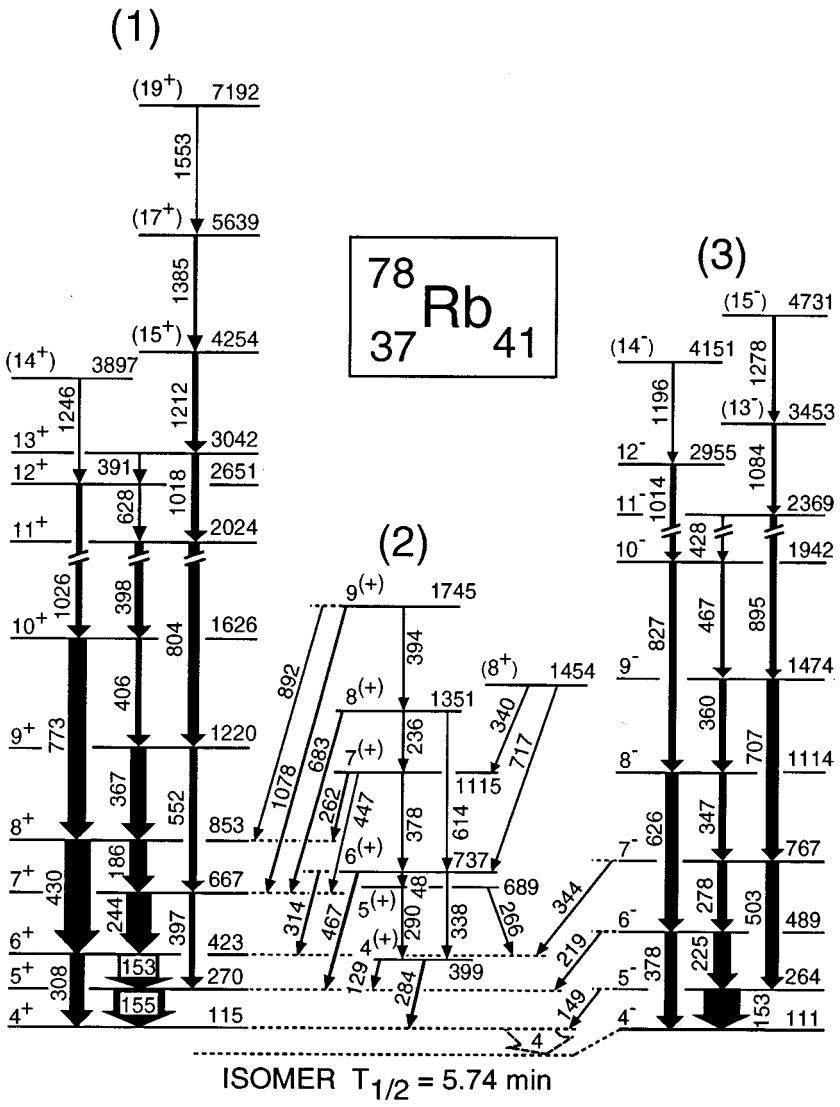

FIG. 1. Partial level scheme of ^{78}Rb showing bands 1–3 which decay into the 4^- isomer. The energy scale has been compressed by a factor of 3 above 2000 keV. The 4 keV transition has been exaggerated for clarity.

larity of $M1$ based on the measured internal conversion coefficient of 0.10 ± 0.02, in good agreement with Ref. [17]. A second decay branch was also found, consisting of a 64.4 keV ($M3$) transition from the isomer to a spin $1\hbar$ state, followed by a known [17] 46.8 keV ($E1$) transition to the ground state. Their work suggests that the parity of the ground state is opposite to that of the isomeric state.

Definite spins of 0 for the ground state and $4\hbar$ for the isomer have been assigned [20,21] in atomic beam experiments. Parities of $0^{(+)}$ and $4^{(-)}$ have been suggested based on the β^+ decay patterns [17]. Relatively strong β branches were seen from the $I=4$ isomer to the lowest 3^- ($\log ft$ = 6.9), 4^- (6.1), and 5^- (6.5) states in ^{78}Kr. In particular the strength of the β branch to the 4^- state is almost within the limits ($\log ft \leqslant 5.9$ [32]) which would exclude forbidden decay and provide a firm assignment of negative parity. Furthermore, the measured magnetic moment of the 4^- isomer, $\mu_I=2.56\mu_N$ [20,21], agrees well with that calculated for the 4^- configuration using the Nilsson orbitals $\pi\frac{5}{2}^+[422]\otimes\nu\frac{3}{2}^-[301]$ proposed by Ekström *et al.* [21].

An assignment of 0^+ is favored for the ground state of ^{78}Rb since a 0^- assignment would permit a first-forbidden unique β^+ decay to the 2_1^+ level of ^{78}Kr, which was not seen [17]. Although $\log ft$ values are not available for the β^+ decay of the ^{78}Sr 0^+ ground state [33,34], a previous study [33] indicates a 103.5 keV line as the strongest γ ray following ^{78}Sr β^+ decay. This is consistent with the picture of positive parity for the ground state and the 103 keV state. Finally, the assignments of 0^+ and 4^- agree with the assignment mentioned above of opposite parity for the two states based on the electromagnetic decays of the isomer.

B. The yrast positive-parity band: Band 1

In all previous level schemes, the most strongly populated bands (1 and 3 in Fig. 1) shared a common 153 keV transition leading to the 4^- isomer. This connection and the measured angular distributions implied that the two bands must have the same parity, in contradiction to the established systematics. This fact and the curious lack of a $7\rightarrow5$ transition in the yrast band (1 in Fig. 1) of previous level schemes prompted a reexamination of intensity balances and coincidence relationships associated with the band. One clue was revealed by a gate on the 186 keV transition, shown in Fig. 3(a), in which the 155 keV line is approximately 15% more

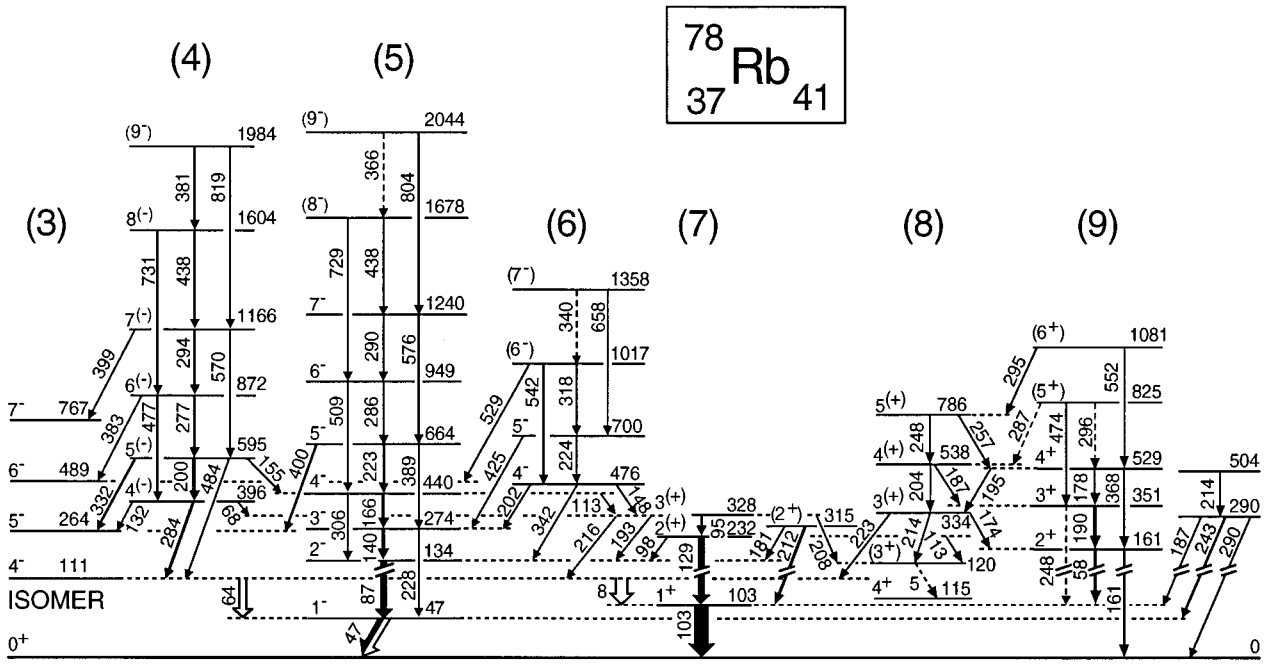

FIG. 2. Partial level scheme of ^{78}Rb showing bands 4–9. The isomeric decays are from Ref. [24]. Above an excitation energy of 111 keV, the scale has been compressed by a factor of 3. For clarity, transitions with energy $<$ 10 keV have been exaggerated and the position of the 1^+ 103 keV state has been shifted closer to the ground state.

intense than the 153 keV decay, and internal conversion decay cannot account for the discrepancy [35]. A reversal of the ordering of these two lines would have other implications including a second 153 keV line in band 3, so a further search was made for more evidence to distinguish between the two possible orderings of the 153 and 155 keV lines.

The most obvious test for a 153 keV doublet would be to look for differences in the two energies, but even with the LEPS detector, gates in bands 1 and 3 show peaks differing by at most 0.1 keV, which is within the measurement uncertainty. Clear evidence comes from decays from the newly discovered band 2 to band 1. Two of these decays (129 and 467 keV) would not fit the previous level scheme. For example, the 155 keV peak is much stronger than the 153 keV line in the 467 keV gate, as shown in Fig. 3(b). This would not be possible if the 153 keV decay were below the 155 keV transition. [The weaker 153 and 225 keV lines in Fig. 3(b) come from coincidences with another 467 keV transition in band 3.]

The new ordering of the 155 keV line below the 153 keV line in band 1 of Fig. 1 makes the energy of the missing $7^+ \rightarrow 5^+$ decay 397.2 keV, which is very close to that of the previously known $11^+ \rightarrow 10^+$ transition. The present data show clear evidence for such a doublet. A peak at 397.2 keV was observed in the spectrum gated on the 804 keV transition where the $11^+ \rightarrow 10^+$ line should not be visible, while a 398.1 keV peak was seen in the 244 keV gate where a possible $7^+ \rightarrow 5^+$ decay should not be visible. A spectrum gated on the 398 keV doublet, shown in Fig. 4, shows both the 804 keV line and a 398 keV peak in coincidence with itself. The measured DCO ratios listed in Table I are also quite different for the two members of the doublet. The lower $7^+ \rightarrow 5^+$ transition was observed but not placed in the level scheme in an earlier work [22] which only reached states up to $9\hbar$ and

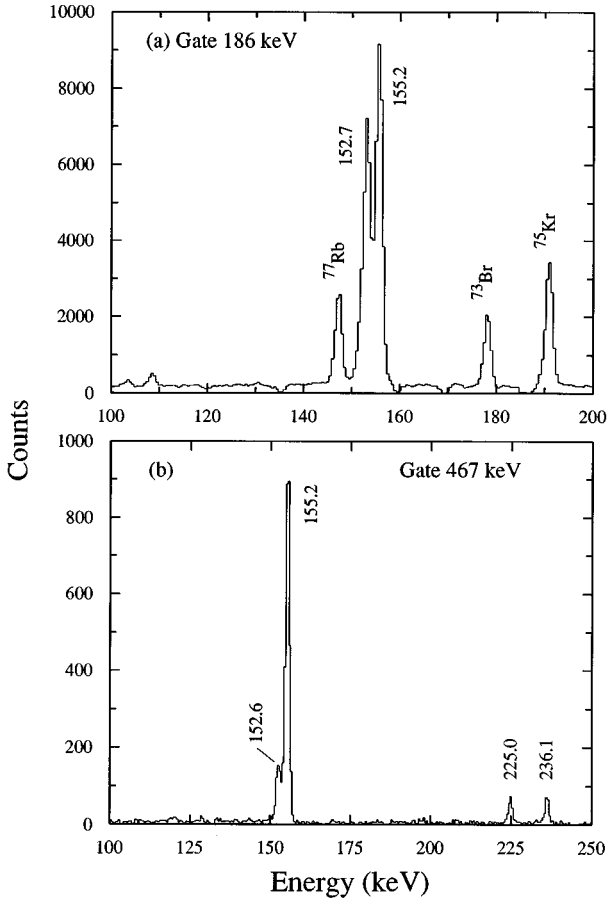

FIG. 3. (a) A portion of the gated spectrum of the 186 keV transition as observed in the ^{54}Fe(^{28}Si,3pn) reaction. (b) A portion of the spectrum projected from a gate on 467 keV, as observed in the ^{58}Ni(^{23}Na,2pn) reaction.

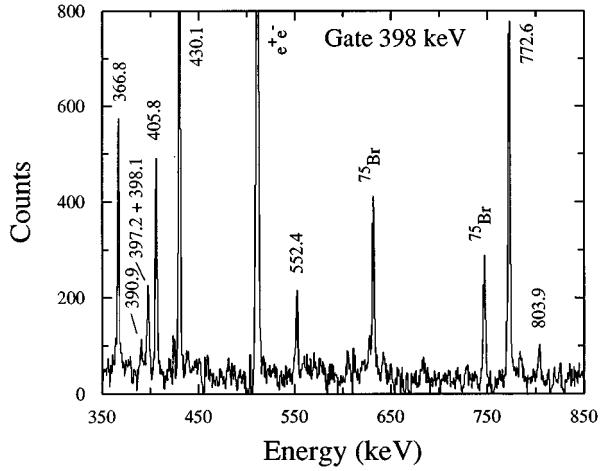

FIG. 4. A portion of the spectrum resulting from a 2 keV wide gate centered on 398 keV, as observed in the ^{54}Fe(^{28}Si,3pn) reaction.

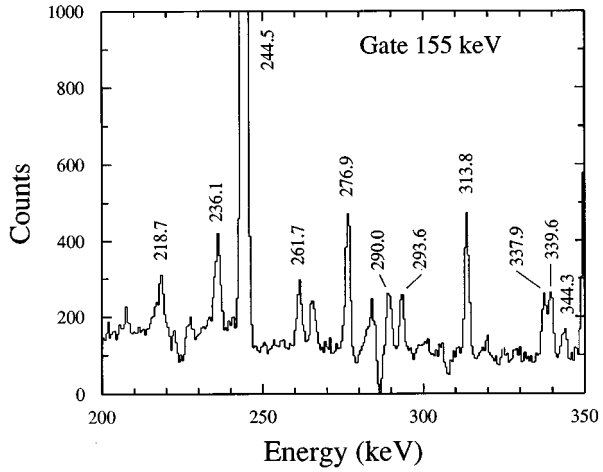

FIG. 6. A portion of the gated spectrum of the 155 keV transition as observed in the ^{58}Ni(^{23}Na,2pn) reaction.

reported a 397.5 keV line with an anisotropy characteristic of $\Delta I=2$ decay.

Even after this rearrangement of the level scheme, different parities would not be likely for bands 1 and 3 if the 308 and 378 keV transitions both end on the same isomeric state (as has previously been assumed), since both have DCO ratios characteristic of $\Delta I=2$ decay and almost certainly $E2$ character. The possibility of separate, but very close, 4^- and 4^+ bandheads is suggested by the behavior of similar states in ^{76}Rb and ^{80}Rb, as shown in Fig. 5. Since their ordering reverses from $A=76$ to 80, an interpolation suggests the two states might be very close together in ^{78}Rb. This observation motivated a search for a low-energy $4^+\rightarrow 4^-$ decay line in the LEPS-γ coincidences. No candidate was found down to the threshold of about 10 keV. However, a careful examination of the γ-γ coincidences did reveal three previously unknown weak linking transitions of energy 148.9, 218.7, and 344.3 keV from band 3 to 1. Figure 6 shows the 218.7 and 344.3 keV lines in a gate on the 155 keV transition. The three linking transitions fix the head of band 1 3.7 keV above that of band 3 and thus prove the existence of two separate bandheads. A highly converted decay of 3.7 keV, which would be very difficult to observe directly, is expected between the two bandheads and is shown with a dashed arrow in Fig. 1. A mean lifetime of about 7 μs is estimated for the 4^+ state assuming an internal conversion coefficient of 110 (arising from $L+M$ shell contributions) and a $B(E1)$ strength of 10^{-5} Weisskopf units (W.u.). Direct decays to states below the isomer are predicted to have partial lifetimes of 11 or more orders of magnitude longer due to the large spin changes.

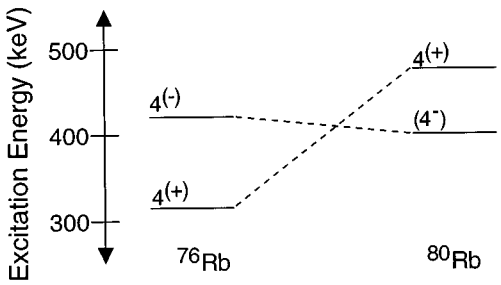

FIG. 5. A comparison of the lowest 4^+ and 4^- states in ^{76}Rb [6] and ^{80}Rb [7].

Band 1 has been observed to spins of $(14)\hbar$ and $(19)\hbar$ at 3897 and 7192 keV, respectively. The measured DCO ratios establish the relative spins in the band up to the 12^+ and 13^+ states. Figure 7 shows a sum of coincidence spectra and contains most of the transitions in this decay chain.

The spins in band 1 are based on the spins in band 3, which are well determined since they are based on the established $I=4$ isomer. The DCO ratios of the 219 and 344 keV decays from band 3 to band 1 imply a spin change of $1\hbar$, and yrast arguments rule out the possibility that the lower states would have the higher spins. This fixes the spins in band 1 to the values shown in Fig. 1. The parity of band 1 could not be determined directly because it was not possible to measure the polarizations of the weak linking transitions. However, all the systematics clearly point to positive parity. The yrast bands of other neighboring odd-odd nuclei have positive parity and appear to be based on the $(\pi g_{9/2}\otimes \nu g_{9/2})$ configuration. The yrast band in ^{78}Rb is quite similar in many respects to those of its neighbors (see Sec. V) and therefore is also expected to have positive parity.

C. The yrast negative-parity band: Band 3

A second band with complementary signature partners had been previously suggested [22,23] to decay directly to the 4^- isomer. Connecting transitions found in the current investigation now firmly base this band (3 in Fig. 1) on the isomer. A second 153 keV transition, separate from the $6^+\rightarrow 5^+$ band 1 transition, remains as a direct decay to the isomer based on its strong coincidence with other members of the band. This band has been observed up to the 4151 keV (14^-) and 4731 keV (15^-) states. Figure 8 shows a sum coincidence spectra consisting of gates set on some of the stronger transitions in the cascade.

Spins and parities have been firmly assigned to this band based on DCO ratios, angular distributions, and linear polarizations. The DCO ratio of the 153 keV decay of the 264 keV level (as measured in several intraband $E2$ gates) is

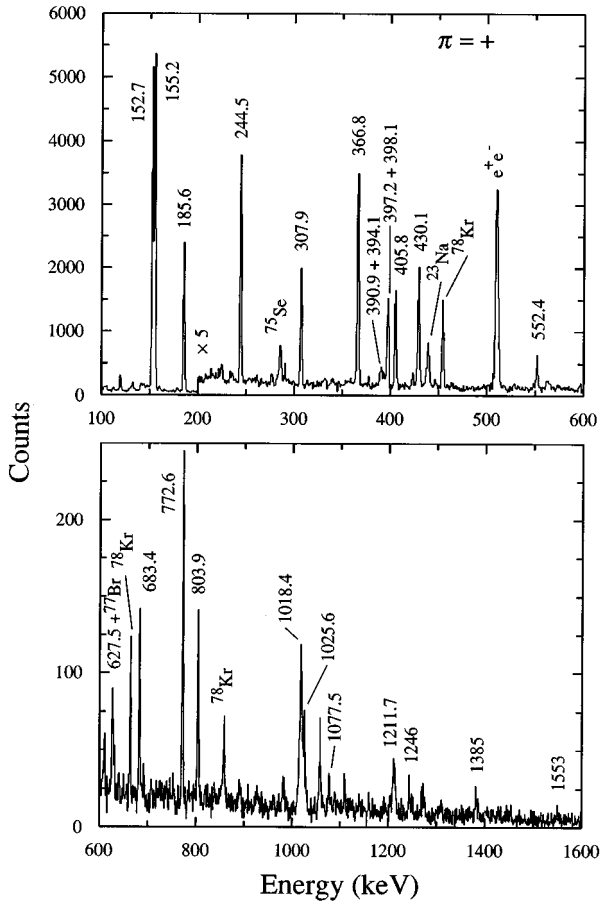

FIG. 7. The sum of 90° spectra gated on the 244, 308, 367, 398, 430, and 804 keV transitions in band 1 observed from the ^{58}Ni(^{23}Na,2pn) reaction showing coincidences with transitions in bands 1 and 2. The number of counts have been multiplied by a factor of 5 for transitions with 200 keV $\leq E_\gamma \leq$ 600 keV.

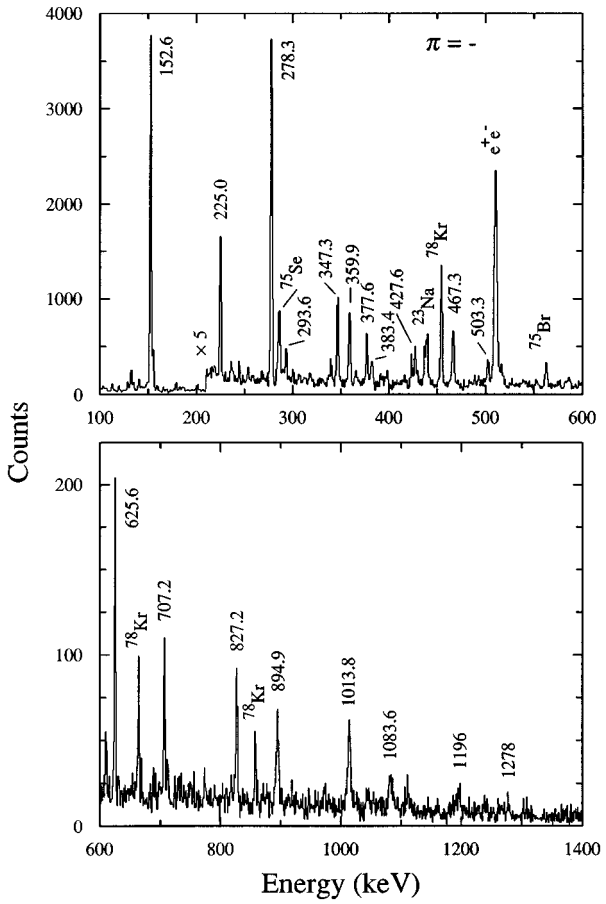

FIG. 8. The sum of 90° spectra gated on the 225, 378, 503, 626, 707, and 827 keV transitions in band 3 showing coincidences with transitions in bands 3 and 4, as observed in the ^{58}Ni(^{23}Na,2pn) reaction. Note the magnification of the intensity scale near 200 keV.

consistent with a $\Delta I=1$ transition. Both the DCO ratio and the angular distribution of the 378 keV decay of the 489 keV level are consistent with a $\Delta I=0$ or $\Delta I=2$ decay, but not with a $\Delta I=1$ decay (unless the mixing ratio $\delta<-0.2$). Furthermore, the measured linear polarization of the 378 keV γ ray supports a transition that does not change parity ($M1$, $E2$) and excludes a parity-changing transition ($E1$, $M2$). Figure 9 shows these conclusions graphically through a χ^2 fit of experimental versus theoretical angular distributions [Fig. 9(a)] and by theoretical polarizations compared with the accepted range of measured polarizations [Fig. 9(b)]. The theoretical values are determined as a function of the mixing ratio and depend on the angular distribution coefficients a_2 and a_4 as well as the initial and final spins of the 378 keV decay, as indicated in the figure. Thus band 3 is a negative-parity band built on the 4^- isomer and the two most strongly populated bands in ^{78}Rb have opposite parity, as in many other $A\approx 80$ nuclei.

D. Negative-parity bands 4, 5, and 6

Three new bands which show mixing between themselves and band 3 have been discovered from the coincidence data. The first is a band built on a $4^{(-)}$ state at 395.6 keV excitation energy and labeled 4 in Fig. 2. Its position in the level scheme is fixed by a number of connecting transitions to band 3. Within the band, the angular distributions of the 199.7 and 570.5 keV lines and the DCO ratios of the 199.7, 276.9, 293.6, 437.8, 570.5, and 818.7 keV decays establish the relative spins shown in the level scheme. The angular distributions and DCO ratios of the 284.4, 331.5, and 383.4 keV decays to band 3 are all characteristic of either $\Delta I=0$ or $\Delta I=2$ transitions, while the DCO ratio of the 131.8 keV line implies a $\Delta I=1$ decay. These are consistent with bandhead spins of either $4\hbar$ or $6\hbar$ for the 395.6 keV level. The latter possibility would make this very weakly populated band yrast and hence conflict with the spin structure of band 3. Thus $I=4$ is assigned to the bandhead at 395.6 keV. Negative parity is very likely because all the decays out of this band go to negative-parity states.

Another new band (5 in Fig. 2) is built on the previously known 46.8 keV $1^{(-)}$ level [24], whose mean life of 610 ns was measured in the present work (see Sec. IV A). The coincidence relations between the 46.8 keV line and others in the band were established in the ^{58}Ni(^{23}Na,2pn) experiment which included a LEPS detector and an expanded ($\approx$800 ns) coincidence time window. Many of the lines in band 5 can be seen in Fig. 10 which is gated on the 46.8 keV γ ray in the LEPS projection of the delayed LEPS-HPGe matrix. The

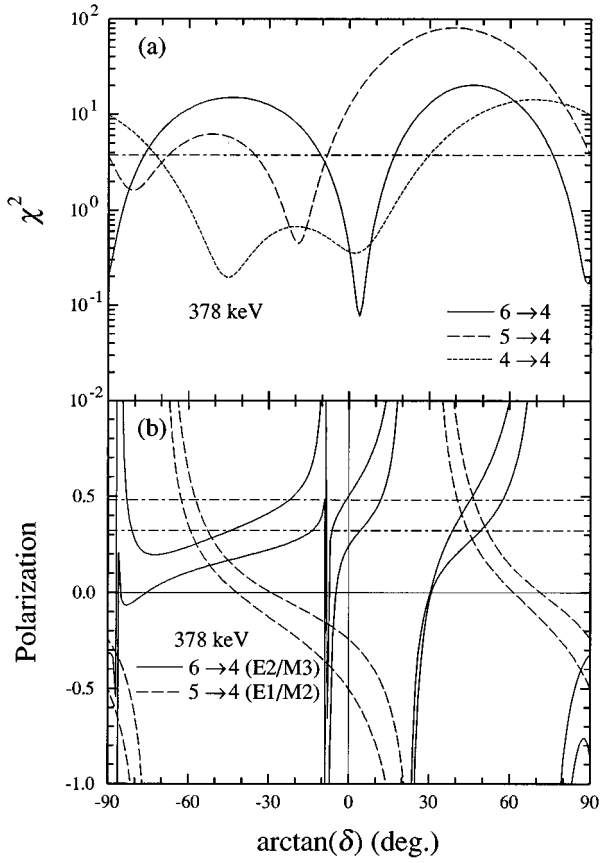

FIG. 9. (a) Graph of χ^2 vs arctan(δ) for the given initial and final spin states of the 378 keV transition. The horizontal dash-dotted line represents the 0.1% confidence limit. (b) Theoretical polarizations, as a function of the mixing ratio, for the given initial and final spin states of the 378 keV transition. The two horizontal dash-dotted lines represent the experimental polarization with its uncertainty.

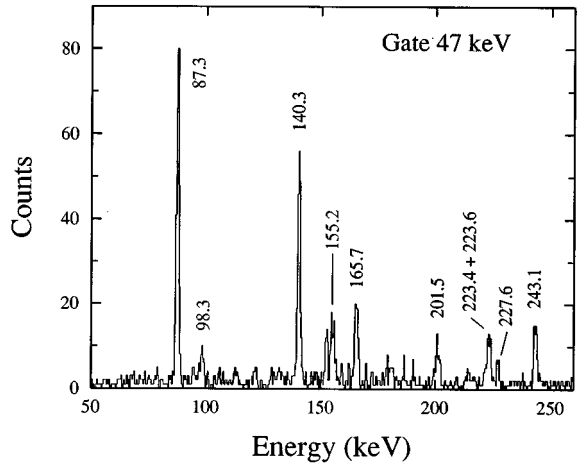

FIG. 10. A portion of a spectrum obtained by gating on the 47 keV transition in the LEPS projection of a LEPS-HPGe delayed coincidence matrix from the ^{58}Ni(^{23}Na,2pn) reaction. An expanded coincidence time window ($\approx$800 ns) was used to observe decays from longer-lived states.

155.2 and 484.1 keV decays from the 595.3 keV state to the 440.1 keV 4^- state in this band and to the 4^- isomer fix the position of the isomer at 111.2 keV, in agreement with Ref. [24]. The energy of the 440.1 keV state is determined both by its decay down this band to the 46.8 keV level and by its decay via a 112.6 keV transition to a 327.5 keV level of band 7 built on the 103.2 keV 1^+ level. The spins in band 5 up through the 7^- level are determined by DCO ratios. Negative parity has been assigned for this band based on the discovery of a 227.6 keV transition between the 3^- 274.4 keV state and the 1^- 46.8 keV state.

The formation of a band based on the 475.9 keV state has also been observed. The relative placement of this sequence (6 in Fig. 2) was determined by the 148.4, 201.5, and 341.8 keV decays from the 475.9 keV level to other established structures, the 528.6 keV transition from the 1017.4 keV state to the 488.8 keV state in band 3, and the 425.1 keV transition from the 699.5 keV state to the 274.4 keV state in band 5. The 425.1 and 341.8 keV decays assign negative parity to this band since they are $\Delta I=2$ transitions terminating on states with known negative parity. Spin assignments were derived from the DCO ratios of the linking transitions to other bands and from the systematics implied by the DCO ratios of the intraband decays.

E. Additional low-spin states

Several new low-spin states have been assigned to ^{78}Rb. Most of these states eventually decay to the ground state. A few states decay by γ rays which were seen previously from studies of the β^+ decay of ^{78}Sr [33,34]. Several of these transitions have now been placed as the decays of the 289.9, 315.4, and 504.0 keV levels. There are several more states which form 3 decay sequences or bands labeled 7, 8, and 9 in Fig. 2. The relative placements of these structures were fixed by several linking transitions found from the coincidence relationships, thus providing more links between the high-spin cascades and the ground state. DCO ratios from several transitions determined the spin assignments for these states, although some remain tentative due to unattainable DCO ratios for some transitions. Positive parity has been assigned to band 9 based on the $E2$ nature of the 160.7 keV decay to the 0^+ ground state. Several decays are observed between bands 8 and 9, strongly suggesting positive parity for band 8 as well.

A new level at 119.7 keV has been introduced based on the 214.5 keV decay of the 334.2 keV state in band 8 and the 112.7 and 207.8 keV decays of the 232.4 and 327.5 keV states, respectively, in band 7. A spin of $I=3$ has been suggested based on the DCO ratio of the 214.5 keV γ ray and the lack of an observed transition from this level to the ground state. Since the transitions which feed into this state originate from probable positive-parity levels and since no decay was seen to the 46.8 keV 1^- state, positive parity is likely for this level. The deexcitation of this state would be very difficult to observe since a decay to any of the known lower-lying levels would be highly converted. However, a calculation of the partial lifetimes indicate that a 4.8 keV transition to the 114.9 keV 4^+ state is the most likely possibility, assuming positive parity for the 119.7 keV state.

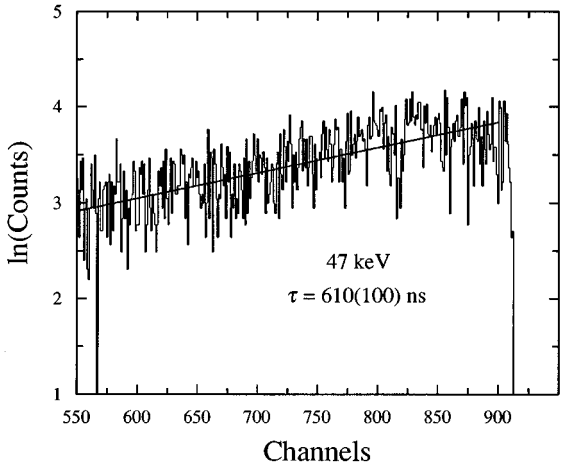

FIG. 11. A portion of the TAC spectrum generated by a gate set on the 47 keV transition in the LEPS projection of a matrix consisting of LEPS energy vs LEPS-HPGe time differences. The solid line shows the least-squares fit of the data for the indicated range of channels. The indicated error in the lifetime reflects statistical errors and systematic errors due to background subtraction and fitting range selection.

IV. LIFETIME MEASUREMENTS AND TRANSITION STRENGTHS

A. Lifetimes from direct timing

The lifetime of the 1^- 46.8 keV state in ^{78}Rb was determined using delayed coincidences measured in the ^{58}Ni(^{23}Na,$2pn$) reaction. The time spectrum was projected from the LEPS-TAC matrix for a 46.8 keV gate on the LEPS spectrum. This decay curve is shown in Fig. 11, where a logarithmic ordinate scale has been used to convert the exponential decay into a linear function of time. The best fit straight line is also shown in the figure. No feeding correction was made because the 87.3 keV feeding transition appears prompt on the nanosecond time scale of the LEPS-TAC matrix and feeding from the 4^- isomer is infinitely long on this time scale. The slope of the best fit line gives a mean lifetime of 610(100) ns for the 46.8 keV level. As a check for any possible systematic errors, the lifetime of the 66.5 keV $3/2^-$ state in ^{77}Kr, populated via the $3pn$ channel, was remeasured to be 170(8) ns, in excellent agreement with Ref. [36].

B. Lifetimes from the Doppler-shift attenuation method

Lifetimes of 12 higher-lying states were determined by applying the Doppler-shift attenuation method (DSAM) to the experimental 145° line shapes generated from both the ^{58}Ni(^{23}Na,$2pn$) and the ^{54}Fe(^{28}Si,$3pn$) data sets. The DSAM involves a comparison of the decay time of the recoiling nuclei with their slowing-down time in the target. This comparison was carried out using a computer simulation code [29] which integrates over the thickness of the target and determines the distribution of recoil velocities at the time of decay as well as the deceleration of the beam as it travels through the target. It corrects for feeding from known higher-lying states and the continuum, as well as for finite detector solid angle and resolution and the energy dependence of the reaction cross sections. A theoretical line shape is generated for each of a range of lifetimes and compared with the measured backward coincidence spectrum to find the best fit. The nuclear and electronic stopping powers used were those suggested by Ziegler *et al.* [37].

The 145° line shapes were obtained from coincidence spectra gated on transitions below the transition of interest. Initially, an upper-limit effective lifetime was determined for the highest state in each cascade for which statistics provided an adequate line shape. The determination of all other lifetimes used these effective lifetimes in addition to direct feeding from in-cascade transitions and side feeding from unknown states as corrections for the fitting process. Side-feeding times were determined from the convention adopted by Moore *et al.* [29] where the highest measurable state for which a mean lifetime can be determined is given a short side-feeding time with an increase of about 0.04 ps per MeV of deexcitation thereafter. In this vein, the present study has incorporated a side-feeding time of 0.05 ps for the (15^+) state, with all other side-feeding times based on this value.

The uncertainty of the lifetime values was determined by finding the values of τ above and below the best fit value which increased the goodness of fit χ^2 per degree of freedom (χ^2_ν) by one unit. Examples of three line-shape fits from the ^{58}Ni(^{23}Na,$2pn$) data are presented in Fig. 12, showing the best fits and the $\chi^2_{\nu,\min}+1$ fits. Table III gives the extracted lifetimes, showing the values obtained for each of the two reactions. The accepted lifetime $\tau_{\rm acc}$ of each state was determined by using a weighted average of the two measurements which favored the ^{58}Ni(^{23}Na,$2pn$) results (see Table III), due to the higher degree of accuaracy expected from the cleaner experimental line shapes observed in this reaction.

Unfortunately, a lifetime could not be determined for the 12^+ state, due to interference from the nearby 1018 and 1020 keV (^{76}Kr contaminant channel [38]) lines. Moreover, the 628 keV line depopulating the same state could not be fitted because its Doppler shift was too small to observe.

C. Transition strengths

The electric quadrupole transition strengths $B(E2)$ were determined from the lifetimes given in Table III and were used to calculate transition quadrupole moments $|Q_t|$ from the rotational model according to

$$Q_t^2=\frac{16\pi}{5}\langle IK20|I-2K\rangle^{-2}B(E2, I\rightarrow I-2). \qquad (3)$$

A value of $K=4$ was used for both bands (1 and 3) from which lifetimes could be measured. From the Q_t values, quadrupole deformations β_2 were inferred, assuming axial symmetry, using

$$\beta_2=\sqrt{\frac{49\pi}{80}+\frac{7\pi Q_t}{6eZr_0^2A^{2/3}}}-\sqrt{\frac{49\pi}{80}}, \qquad (4)$$

where $r_0=1.2$ fm. Most magnetic dipole transition strengths $B(M1)$ were calculated using a quadrupole-dipole mixing ratio of $\delta=0$ since $B(M1)$ values are rather insensitive to δ as long as it is small. However, a mixing ratio for the 406 keV line was determined from the angular distribution experiment and was used to calculate a $B(M1)$ as well as a

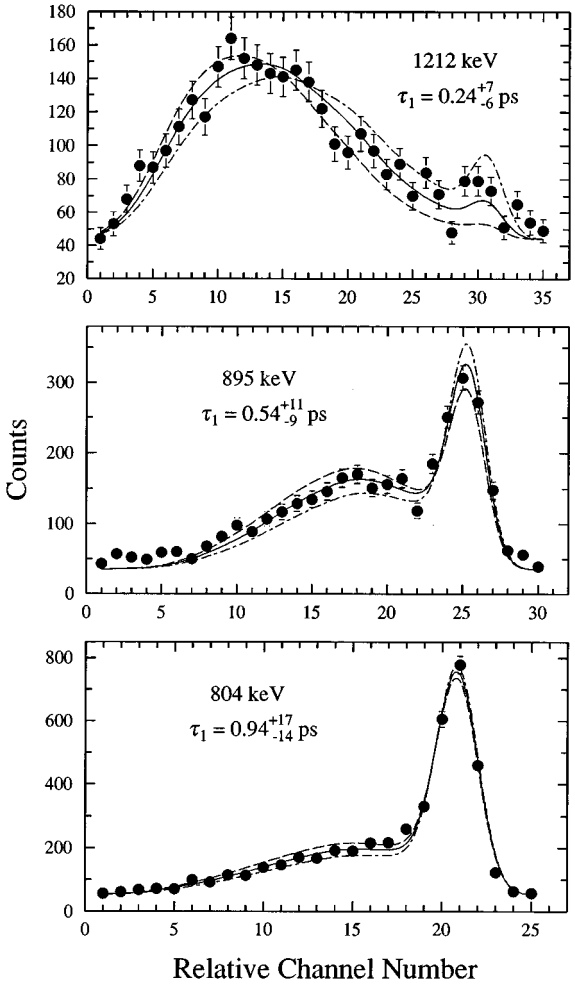

FIG. 12. Examples of the best fit (solid curve) and $\chi^2_{\nu,\min}+1$ fits (broken curves) to the 145° experimental line shapes using the Doppler-shift attenuation method.

$B(E2)$ for this transition. All measurable transition strengths, Q_t, and β_2 values are given in Table III. The branching ratios used in the calculation of these quantities were the result of an average of two measurements in which those from the ^{54}Fe(^{28}Si,3pn) reaction were weighted twice as much as those derived from the ^{58}Ni(^{23}Na,2pn) experiment since the statistics of the gates on higher-lying transitions were generally better from the former reaction.

V. DISCUSSION

In general, many similarities can be found between rotational bands in different nuclei if they are built on the same intrinsic qp structure. Such is the case with the positive-parity yrast bands of odd-odd nuclei in the mass 80 region, which are well described theoretically by the occupation of two unlike $g_{9/2}$ nucleons, as discussed in Sec. I. To see how well the positive-parity band in ^{78}Rb (1 in Fig. 1) fits the pattern exhibited by its odd-odd neighbors, several systematic tests have been performed. Unfortunately, the behavior of the negative-parity bands in odd-odd nuclei is not as well understood theoretically because of the complexity of negative-parity single-particle energy levels. Although this complicates any comparisons between negative-parity bands in neighboring nuclei, it is important to study the characteristics of these bands so that a better understanding of their intrinsic structures can be achieved. The lifetime measurements provide a good determination of the degree of collectivity and deformation in the lowest positive- and negative-parity bands (1 and 3) in ^{78}Rb and permit a direct comparison with theoretical predictions.

A. Signature splitting and inversion

One striking feature of almost all odd-odd nuclei in this region is the large signature splitting in the yrast band and a reversal of the splitting pattern near spin $9\hbar$. This effect is clearly seen by plotting the normalized energy differences of adjacent states (which corresponds to a moment-of-inertia parameter) versus the spin of the initial state I_i. Figure 13 displays this information for the yrast band of ^{78}Rb (1 in Fig. 1) along with those of the $N=41$ isotones ^{80}Y [9] and ^{76}Br [3,4], and the $Z=37$ isotopes ^{80}Rb [7,8] and ^{76}Rb [6].

The pattern for each graph in Fig. 13 is essentially the same. At high spins, the odd-spin states (open circles) are relatively lower in energy and the alternations are large, indicating a relatively high degree of signature splitting. At low spins, the even-spin states (filled circles) are lower in energy and the degree of signature splitting is reduced. Near the region of $9\hbar$, there is a reversal in the phase of the pattern. Kreiner and Mariscotti predicted [15] this reversal to occur at $9\hbar$, the maximum spin that can be obtained from the $(\pi g_{9/2}\otimes \nu g_{9/2})$ intrinsic configuration. In their calculation using a two-qp-plus-rotor model applied to ^{76}Br, the total angular momentum below $9\hbar$ is achieved from both collective rotation and realignment of the qp spins, while above $9\hbar$ additional angular momentum is generated from rotation only. In ^{78}Rb, the reversal occurs at spin $10\hbar$, similar to the other nuclei shown in Fig. 13. The small shift of the inversion point is most likely due to a residual proton-neutron interaction, which was shown to be important in odd-odd ^{120}Cs [39]. Since the total spin of two fully aligned unlike $g_{9/2}$ qp has odd spin ($9\hbar$), the high-spin states with odd spin are favored and lie relatively lower in energy.

Although a predictable pattern is observed in the energy spacings of the lowest positive-parity bands of odd-odd nuclei, the same is not true of the lowest negative-parity bands, as seen in a recent survey [40]. This is probably due to the higher density of negative-parity orbitals in this region, yielding many different combinations of negative-parity configurations which themselves can mix with one another. Figure 14(a) displays the energy spacings between adjacent levels as a function of spin for the lowest negative-parity band in ^{78}Rb (3 in Fig. 1). The pattern is significantly different from that seen in band 1 (Fig. 13). Although the odd-spin states (open circles) are still favored at high spins, the signature splitting is less pronounced and there is no indication of a phase reversal. However, it must be stressed that odd-spin states are not always favored at high spins in the lowest negative-parity bands of other neighboring odd-odd nuclei, further confirming the added complexity associated with these bands. The $B(M1)$ strengths for band 3 are shown in Fig. 14(b) for comparison and will be discussed in Sec. V B.

TABLE III. Mean lifetimes of states in ^{78}Rb measured by the Doppler-shift attenuation method and by direct timing, along with transition strengths $B(M1)$ or $B(E2)$, transition quadrupole moments $|Q_t|$, and quadrupole deformations β_2.

I_i^π	E_γ (keV)	τ_1[a,b] (ps)	τ_2[a,c] (ps)	τ_{acc}[d] (ps)	$B(E2)$[e] (W.u.)	$B(M1)$[f] (W.u.)	$\|Q_t\|$ (e b)	β_2[g]
Band 1								
10^+	772.6	1.92^{+40}_{-30}	1.49^{+72}_{-38}	1.78^{+40}_{-30}	70^{+14}_{-13}		2.5(2)	0.30^{+3}_{-2}
	405.8				2^{+3}_{-2}	0.04(1)		
11^+	803.9	0.94^{+17}_{-14}	0.86^{+20}_{-16}	0.91^{+17}_{-14}	69^{+12}_{-11}		2.4(2)	0.29(2)
	398.1					0.27(5)		
13^+	1018.4	0.36^{+11}_{-9}	0.48^{+12}_{-10}	0.40^{+11}_{-9}	74^{+21}_{-16}		2.3(3)	0.28^{+4}_{-3}
	390.9					0.29^{+12}_{-10}		
(14^+)	1246	< 0.26[h]	< 0.42[h]	< 0.31[h]	> 44		> 1.7	> 0.22
(15^+)	1211.7	0.24^{+7}_{-6}	0.13^{+9}_{-6}	0.20^{+7}_{-6}	79^{+34}_{-20}		2.3^{+4}_{-3}	0.28^{+5}_{-3}
(17^+)	1385	< 0.17[h]	< 0.20[h]	< 0.18[h]	> 45		> 1.7	> 0.21
Band 3								
10^-	827.2	0.84^{+16}_{-13}	0.97^{+71}_{-31}	0.88^{+16}_{-13}	93^{+16}_{-14}		2.8(2)	0.34^{+3}_{-2}
	467.3					0.08(2)		
11^-	894.9	0.54^{+11}_{-9}	0.61^{+10}_{-8}	0.56^{+10}_{-8}	106^{+18}_{-16}		2.9(2)	0.35^{+3}_{-2}
	427.6					0.12^{+4}_{-3}		
12^-	1013.8	0.40^{+10}_{-9}	< 0.64[h]	0.40^{+10}_{-9}	96^{+28}_{-19}		2.7^{+4}_{-3}	0.33(4)
(13^-)	1083.6	0.25^{+8}_{-7}	< 0.45[h]	0.25^{+8}_{-7}	110^{+43}_{-27}		2.8^{+5}_{-4}	0.34^{+5}_{-4}
(14^-)	1196	< 0.34[h]		< 0.34[h]	> 50		> 1.8	> 0.23
(15^-)	1278	< 0.26[h]		< 0.26[h]	> 46		> 1.8	> 0.22
Band 5								
1^-	46.8	610(100)[i]		610(100)[i]		$4.8^{+9}_{-7}\times 10^{-6}$ [j]		

[a]Measured using the Doppler-shift attenuation method unless otherwise noted.
[b]Determined from the ^{58}Ni(^{23}Na,$2pn$) reaction.
[c]Determined from the ^{54}Fe(^{28}Si,$3pn$) reaction.
[d]$\tau_{acc}=(2\tau_1+\tau_2)/3$ as explained in the text.
[e]1 W.u. = 19.8 e^2 fm^4.
[f]The quadrupole-dipole mixing ratio δ was assumed to be zero unless it was determined experimentally (Table II). 1 W.u. = 1.79 μ_N^2.
[g]Assuming axial symmetry.
[h]Effective lifetime limit.
[i]Measured by direct timing in units of ns.
[j]$B(E1)$ in W.u. 1 W.u. = 1.18 e^2 fm^2.

B. Transition strengths and collectivity

The electric quadrupole transition strengths $B(E2)$ were calculated using the adopted lifetimes τ_{acc}. Both quantities are given in Table III. An examination of the $E2$ strengths reveals strong collective enhancements by factors of 70 to 110 above the single-particle estimate for both bands 1 and 3 in ^{78}Rb. This behavior of the $B(E2)$ rates is well reflected by the transition quadrupole moments Q_t. The experimentally determined Q_t values are shown in Fig. 15 for band 1 (top) and band 3 (bottom), along with theoretical curves which will be discussed in Sec. V D. Both bands exhibit a high degree of collectivity and quadrupole deformation ($\beta_2 \approx 0.3$), with those of band 3 appearing to be slightly higher (see also Table III).

It is also instructive to examine the magnetic dipole transition strengths $B(M1)$. Large $B(M1)$ alternations in the yrast positive-parity band have been directly observed in ^{74}Br [2] and ^{82}Y [10], and can be deduced from large variations in the $B(M1)/B(E2)$ ratios in several other nuclei, since $B(E2)$ values generally remain relatively constant or vary smoothly within a rotational band. The $M1$ strengths in band 1 of ^{78}Rb are shown in Fig. 16 and compared with those of the yrast positive-parity band of ^{82}Y, where a wider range of lifetimes have been measured [14]. Diamond symbols indicate $B(M1)$ values which have been estimated, assuming constant $B(E2)$ strengths, for states in ^{78}Rb from which lifetimes could not be extracted using the DSAM or direct timing. In both nuclei, strong oscillations are seen, with the $M1$ strengths being much larger from states of odd spin to states of even spin than those from even- to odd-spin states. These alternations can be explained [10] using a two-qp-plus-triaxial rotor model in terms of how the unpaired particles couple to the rotating core. A $\Delta I=1$ decay from an odd-spin state involves only a realignment of the single-particle spin without altering the core spin and hence generates strong $M1$ radiation. The corresponding decay beginning from an even-spin state requires a change in the core rotation which leads to reduced $B(M1)$ strength. Below spin $9\hbar$, the alternations in ^{82}Y are reduced, possibly reflecting the change of excitation modes from rotation to qp coupling plus rotation. Although the alternations in ^{78}Rb do not exhibit this change of behavior, it is difficult to draw detailed conclusions since the $B(M1)$ values are only estimates in this spin region. Regardless of the magnitude of the oscilla-

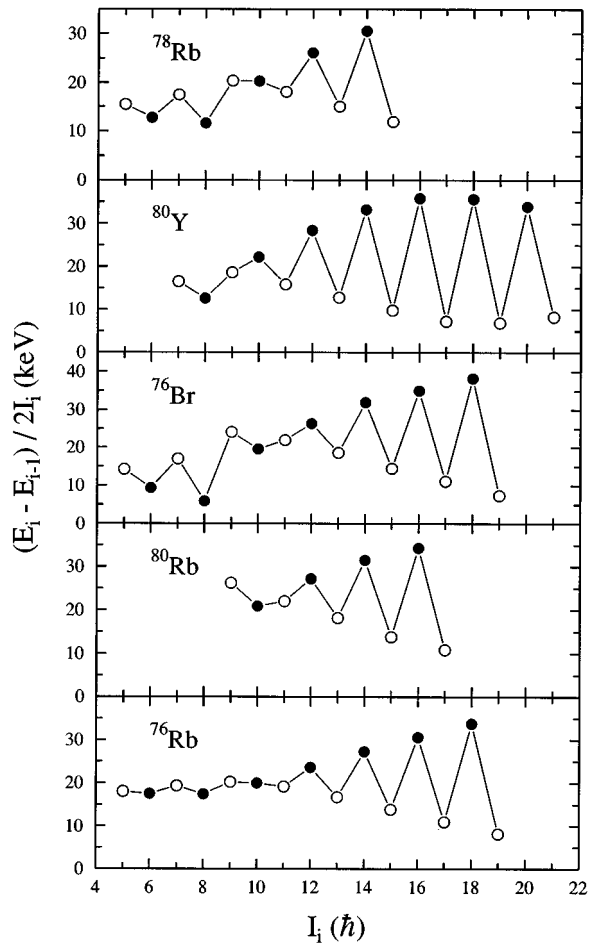

FIG. 13. Normalized energy differences between adjacent levels in the yrast positive-parity bands of ^{78}Rb, the $N=41$ isotones ^{80}Y [9] and ^{76}Br [3,4], and the $Z=37$ isotopes ^{80}Rb [7,8] and ^{76}Rb [6]. States in which the initial state I_i has even (odd) spin are shown with filled (open) circles.

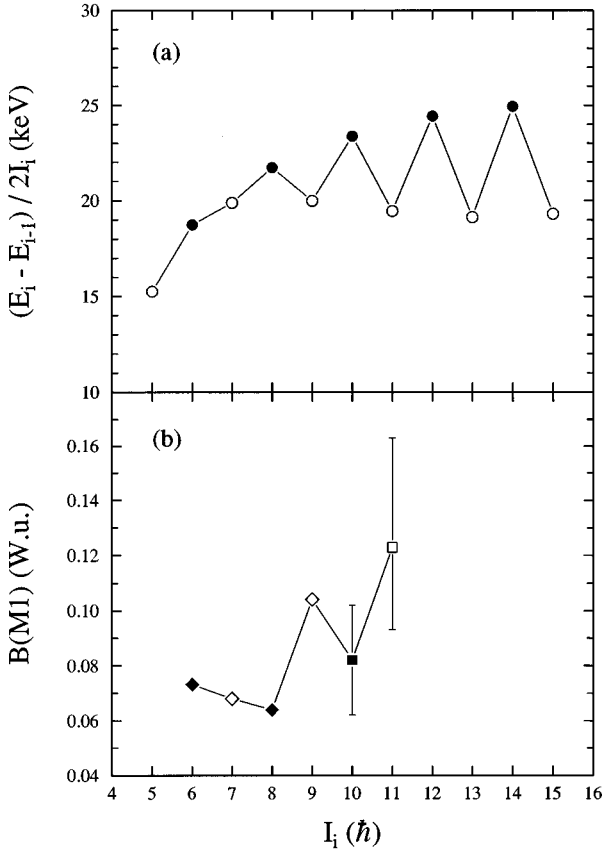

FIG. 14. (a) Normalized energy differences between adjacent levels in the lowest negative-parity band in ^{78}Rb. States in which the initial state I_i has even (odd) spin are shown with filled (open) circles. (b) $B(M1)$ strengths as a function of initial state spin for the lowest negative-parity band in ^{78}Rb. States in which the initial state I_i has even (odd) spin are shown with filled (open) symbols. Squares (diamonds) are used to show $M1$ strengths determined from measured (estimated) lifetimes.

tions, neither graph indicates a phase change near spin $9\hbar$, unlike those observed in Fig. 13. Evidently, the change in the way angular momentum is generated affects the level energies more than the $M1$ strengths.

The measured $B(M1)$ rates of band 3 are displayed in Fig. 14(b) along with estimated values (shown by diamond symbols). There appears to be emerging evidence for an alternation at the point where a regular signature splitting pattern begins [see Fig. 14(a)]. These alternations are similar to those of band 1 in that the odd-spin states produce relatively higher values than those of the even-spin states, although the alternation magnitudes are much weaker than those of band 1. However, more experimental information is needed before firm conclusions can be drawn.

C. Cranked-shell model analysis

The $B(E2)$ values determined for bands 1 and 3 in ^{78}Rb are indicative of the strong collective natures observed in many rotational bands. Thus it is worthwhile to apply the cranking model [41] to these bands to extend the systematics.

The kinematic moments of inertia $J^{(1)}$ for band 1 in ^{78}Rb are compared with those of the yrast positive-parity bands of ^{76}Br [3,4] and ^{76}Rb [6] in Fig. 17. Each graph indicates a very similar pattern for $J^{(1)}$. The values are quite large at low rotational frequencies ω, then drop and saturate to approximately the rigid rotor value of 20 to 25 $\hbar^2$/MeV once ω has exceeded about 0.5 MeV/$\hbar$. This tendency has been observed in a number of odd-odd nuclei in the mass 80 region [16,40]. It is also consistent with the concept of competition between qp alignment and collective rotation generating angular momentum at low spins converting to collective rotation dominating at high spins. The convergence to approximately the rigid rotor value has been related [40] to the disappearance of static pairing at high spins, although it has not as yet been completely explained.

The values of $J^{(1)}$ for band 3 in ^{78}Rb are given in Fig. 18. This band appears to be a good rotor over a range of rotational frequencies as the curves for both signatures vary slowly and smoothly with ω. Other negative-parity bands in ^{78}Rb, such as bands 4, 5, and 6, appear to show signs of rotational structures, but they are not known to very high spins and hence the behavior of their $J^{(1)}$ values is difficult to establish at this time.

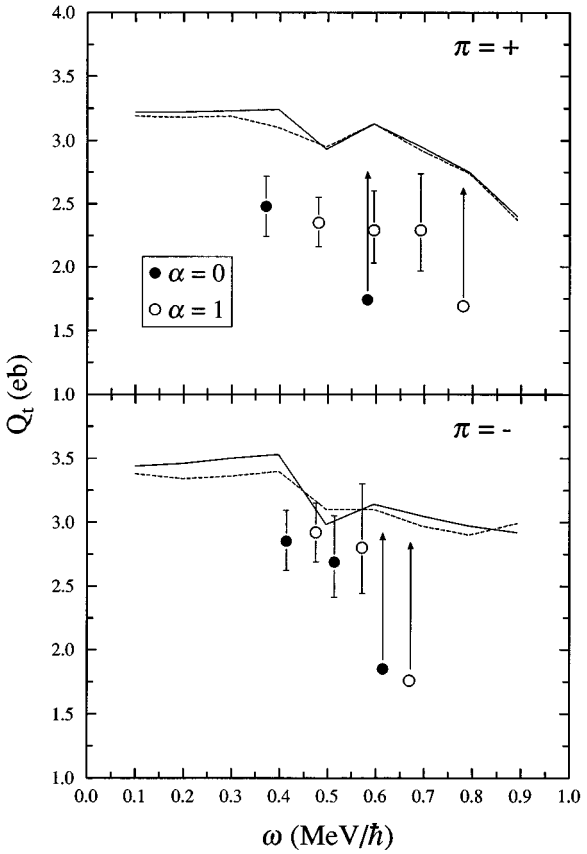

FIG. 15. Theoretical and experimental Q_t values for the lowest positive-parity (top) and negative-parity (bottom) bands in ^{78}Rb. The solid (dashed) curves indicate the theoretical values with signature $\alpha=1$ ($\alpha=0$). Experimental points with arrows indicate lower limits established from effective lifetimes.

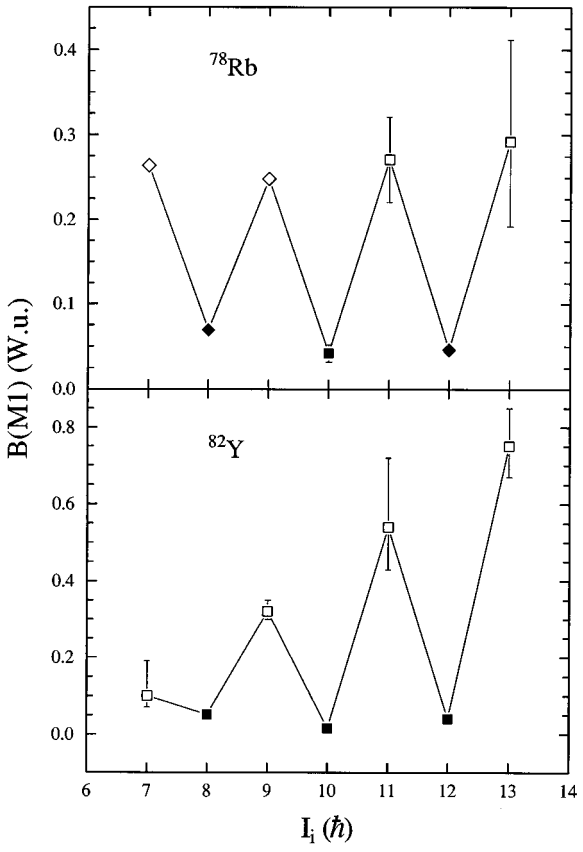

FIG. 16. $B(M1)$ strengths as a function of initial-state spin for the yrast positive-parity bands in ^{78}Rb and ^{82}Y [14]. States in which the initial state I_i has even (odd) spin are shown with filled (open) symbols. Squares (diamonds) are used to show $M1$ strengths determined from measured (estimated) lifetimes. Error bars not shown for any square symbol are smaller than the symbol size.

D. Hartree-Fock-Bogolyubov cranking calculations

Hartree-Fock-Bogolyubov cranking calculations were performed using the Woods-Saxon cranking model [42] and used to generate total Routhian surfaces (TRS) for ^{78}Rb. A short-range monopole pairing force was included, and the cranking approximation was utilized to describe the rotation.

Figure 19 shows four TRS in the (β_2,γ) plane at two different rotational frequencies. At each grid point, the Routhian was minimized with respect to the hexadecapole deformation β_4. The qp labeling scheme of Ref. [43] was used, where lower (upper) case letters are used for the proton (neutron) configuration. Thus the aA case stands for the lowest proton and neutron configuration yielding overall positive parity and signature $\alpha=1$. The aF configuration represents overall negative parity with signature $\alpha=1$.

At a low rotational frequency, $\omega=0.198$ MeV/$\hbar$, both the aA and aF configurations appear to be near-prolate ($\gamma\approx0°$) in shape and well deformed ($\beta_2\approx0.34$). There is almost no change at a higher rotational frequency of $\omega=0.595$ MeV/$\hbar$, although a secondary nearly oblate minimum develops in the negative-parity configuration.

Theoretical Q_t values were calculated as a function of the triaxiality parameter γ (in the high-spin approximation [44,45]), and the charge quadrupole deformation β_2, which has a simple relation [46,47] to the quadrupole deformation of the nuclear matter distribution given by the TRS calculations. The theoretical results are shown in Fig. 15 for the lowest positive- (top) and negative-parity (bottom) states. In each band, the theoretical curves are somewhat higher than the experimental points and tend to be more sensitive to rotational frequency than the experimental points (also shown in Fig. 15), which seem to remain relatively constant. Slightly higher Q_t values are predicted for band 3 compared to band 1, in agreement with the experimental trend.

VI. SUMMARY

High-spin states in ^{78}Rb were examined using the ^{58}Ni(^{23}Na,$2pn$) reaction at 65 and 70 MeV and the ^{54}Fe(^{28}Si,$3pn$) reaction at 120 MeV. Prompt γ-γ coincidences were measured in both experiments using the Pitt-FSU detector array. Since the coincidence runs involved the use of thick targets, lifetimes of several states were determined using the Doppler-shift attenuation method, while a delayed coincidence measurement was used to obtain another lifetime using direct timing. Spins were assigned based on DCO ratios and angular distributions. Linear polarizations of γ rays along with systematic arguments provided the parity assignments.

Several uncertainties in the low-spin region of ^{78}Rb remaining from previous investigations have been resolved in the current study. The two strongest bands, once linked by a

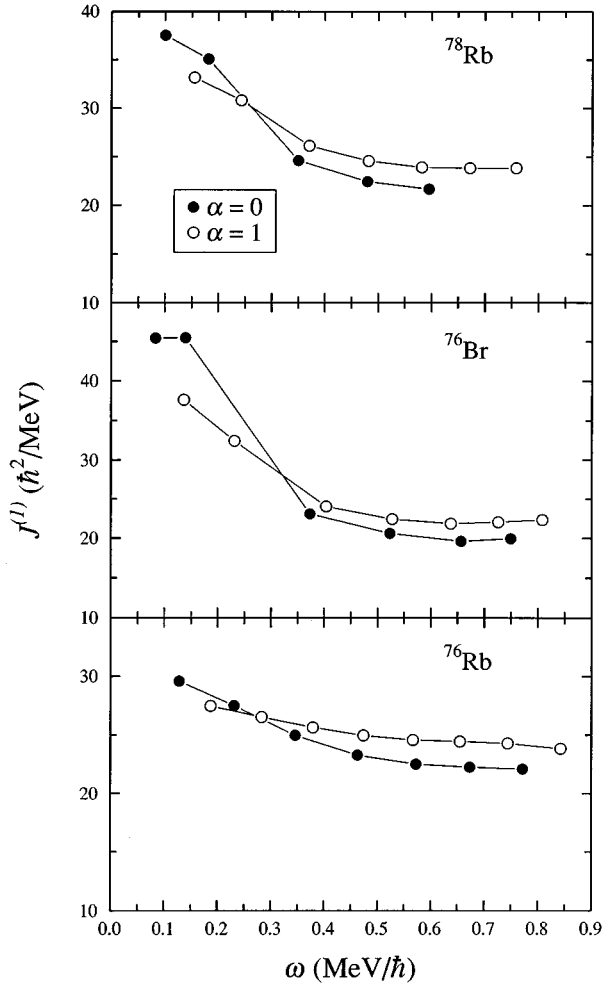

FIG. 17. Kinematic moments of inertia $J^{(1)}$ as a function of rotational frequency ω for the yrast positive-parity bands in ^{78}Rb, ^{76}Br [3,4], and ^{76}Rb [6].

common 153 keV transition and assumed to have the same parity, now have been decoupled such that the yrast band has

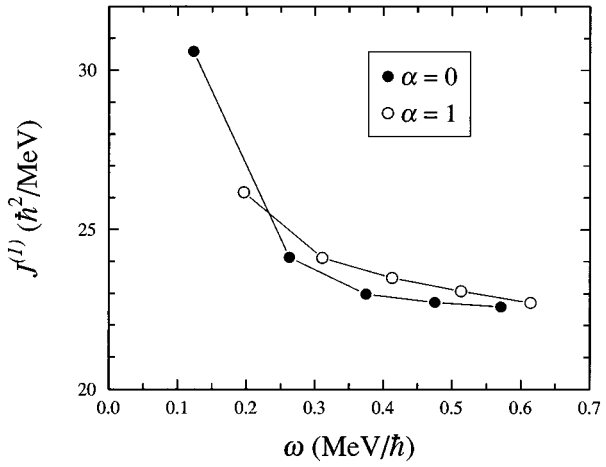

FIG. 18. Kinematic moments of inertia $J^{(1)}$ as a function of rotational frequency ω for the lowest negative-parity band in ^{78}Rb.

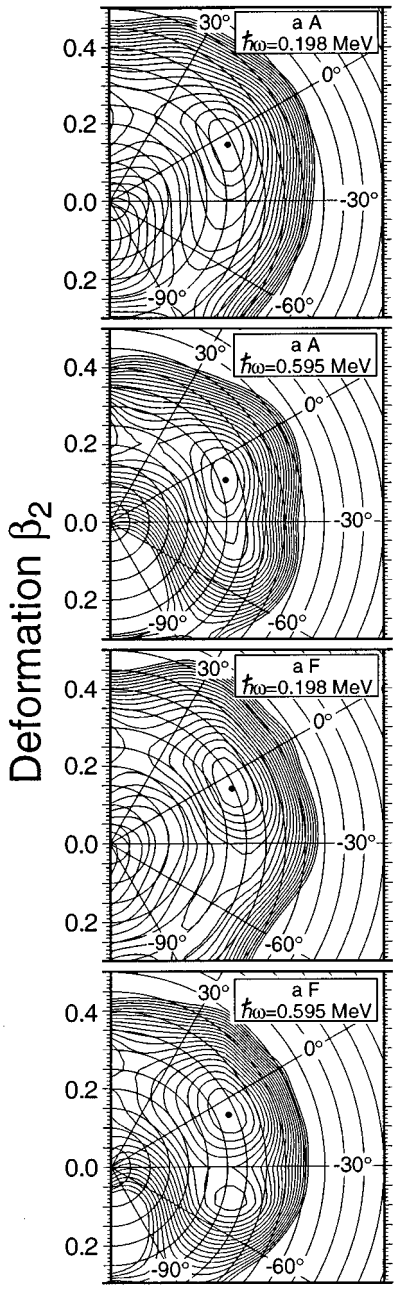

FIG. 19. Sample total Routhian surface plots in the (β_2,γ) polar coordinate plane for ^{78}Rb for two rotational frequencies and two different configurations as indicated in each plot. The aA configuration corresponds to $(\pi,\alpha) = (+,1)$ (odd spins in band 1), and the aF configuration corresponds to $(\pi,\alpha) = (-,1)$ (odd spins in band 3). The spacing between contour lines is 200 keV.

positive parity and the yrare band negative parity. In the process, a 153 keV and a 398 keV doublet have been resolved and placed in the level scheme. Linking transitions between the yrast and yrare bands indicate that the lowest 4^+ and 4^- states are separated by about 4 keV. Several new low-spin states have been observed, some of which provide a direct link from the high-spin states to the ground state and thus fix the position of the 4^- isomer at 111.2 keV.

The yrast band of ^{78}Rb was observed to be very similar to the positive-parity yrast bands of several neighboring odd-odd nuclei. Large signature splittings were observed at high spins followed by a phase inversion near spin $9\hbar$. This re-

versal, which occurs at spin $10\hbar$ in ^{78}Rb, has been attributed to the point at which the generation of angular momentum changes from collective rotation at high spins to rotation and quasiparticle realignment at low spins. A large oscillatory behavior was also seen in the $B(M1)$ strengths, with no indication of a phase inversion. A cranked-shell model analysis indicates a drop in the kinematic moments of inertia to approximately the rigid rotor value (20 to 25 $\hbar^2$/MeV) at high spins. These facts are consistent with a $(\pi g_{9/2} \otimes \nu g_{9/2})$ configuration for the yrast band in ^{78}Rb.

The second-strongest band in ^{78}Rb has negative parity, as in other odd-odd nuclei. Signature splitting in the level energies and $M1$ strengths have been observed in this cascade, but they are not as pronounced as those in the yrast band. Moreover, no consistent pattern has emerged among the odd-odd nuclei for the lowest negative-parity bands because of the larger variety of possible configurations for these bands.

Hartree-Fock-Bogolyubov cranking calculations predict a well-deformed ($\beta_2 \approx 0.34$), near-prolate shape for both the lowest positive- and negative-parity configurations. Transition quadrupole moments Q_t derived from these calculations agree fairly well with those inferred from the lifetime measurements, and both indicate that the negative-parity band is slightly more deformed than the positive-parity band.

ACKNOWLEDGMENTS

We wish to thank W. Nazarewicz for providing his Hartree-Fock-Bogolyubov cranking calculations. We are also grateful to E. G. Myers for his technical support throughout each of the experiments. This work was supported in part by the National Science Foundation.

[1] J. Döring, J.W. Holcomb, T.D. Johnson, M.A. Riley, S.L. Tabor, P.C. Womble, and G. Winter, Phys. Rev. C **47**, 2560 (1993).

[2] J.W. Holcomb, T.D. Johnson, P.C. Womble, P.D. Cottle, S.L. Tabor, F.E. Durham, and S.G. Buccino, Phys. Rev. C **43**, 470 (1991).

[3] S.G. Buccino, F.E. Durham, J.W. Holcomb, T.D. Johnson, P.D. Cottle, and S.L. Tabor, Phys. Rev. C **41**, 2056 (1990).

[4] D.F. Winchell, J.X. Saladin, M.S. Kaplan, and H. Takai, Phys. Rev. C **41**, 1264 (1990).

[5] E. Landulfo, D.F. Winchell, J.X. Saladin, F. Cristancho, D.E. Archer, J. Döring, G.D. Johns, M.A. Riley, S.L. Tabor, V.A. Wood, and O. Dietzsch, Phys. Rev. C **54**, 626 (1996).

[6] A. Harder, M.K. Kabadiyski, K.P. Lieb, D. Rudolph, C.J. Gross, R.A. Cunningham, F. Hannachi, J. Simpson, D.D. Warner, H.A. Roth, Ö. Skeppstedt, W. Gelletly, and B.J. Varley, Phys. Rev. C **51**, 2932 (1995).

[7] J. Döring, G. Winter, L. Funke, B. Cederwall, F. Lidén, A. Johnson, A. Atac, J. Nyberg, G. Sletten, and M. Sugawara, Phys. Rev. C **46**, R2127 (1992).

[8] M.A. Cardona, G. García-Bermúdez, C. Baktash, M.L. Halbert, D.C. Hensley, N.R. Johnson, I.Y. Lee, F.K. McGowan, M.A. Riley, A. Virtanen, V. Abenante, D.G. Sarantites, T.M. Semkow, and H.C. Griffin, in *Nuclear Structure in the Nineties*, edited by N.R. Johnson (Oak Ridge National Laboratory, Oak Ridge, 1991), p. 78.

[9] D. Bucurescu, C.A. Ur, D. Bazzacco, C. Rossi-Alvarez, P. Spolaore, C.M. Petrache, M. Ionescu-Bujor, S. Lunardi, N.H. Medina, D.R. Napoli, M. De Poli, G. de Angelis, F. Brandolini, A. Gadea, P. Pavan, and G.F. Segato, Z. Phys. A **352**, 361 (1995).

[10] P.C. Womble, J. Döring, T. Glasmacher, J.W. Holcomb, G.D. Johns, T.D. Johnson, T.J. Petters, M.A. Riley, V.A. Wood, S.L. Tabor, and P. Semmes, Phys. Rev. C **47**, 2546 (1993).

[11] J. Mukai, A. Odahara, H. Tomura, S. Suematsu, S. Mitarai, T. Kuroyanagi, D. Jerrestam, J. Nyberg, G. Sletten, A. Atac, S.E. Arnell, H.A. Roth, and Ö. Skeppstedt, Nucl. Phys. **A568**, 202 (1994).

[12] G. García-Bermúdez, H. Somacal, M.A. Cardona, A. Filevich, E. Achterberg, and L. Szybisz, Phys. Rev. C **51**, 1181 (1995).

[13] S.D. Paul, H.C. Jain, S. Chattopadhyay, M.L. Jhingan, and J.A. Sheikh, Phys. Rev. C **51**, 2959 (1995).

[14] G.D. Johns, K.A. Christian, R.A. Kaye, S.L. Tabor, G. García-Bermúdez, M.A. Cardona, A. Filevich, H. Somacal, and L. Szybisz, Phys. Rev. C **53**, 1541 (1996).

[15] A.J. Kreiner and M.A.J. Mariscotti, Phys. Rev. Lett. **43**, 1150 (1979).

[16] S.L. Tabor, Phys. Rev. C **45**, 242 (1992).

[17] G.K. Bavaria, J.E. Crawford, S. Calamawy, and J.E. Kitching, Z. Phys. A **302**, 329 (1981).

[18] E. Nolte and Y. Shida, Z. Phys. **256**, 243 (1972).

[19] N.E. Sanderson, J.C. Lisle, and J.C. Willmott, J. Phys. A **7**, 1156 (1974).

[20] C. Thibault, F. Touchard, S. Büttgenbach, R. Klapisch, M. de Saint Simon, H.T. Duong, P. Jacquinot, P. Juncar, S. Liberman, P. Pillet, J. Pinard, J.L. Vialle, A. Pesnelle, and G. Huber, Phys. Rev. C **23**, 2720 (1981).

[21] C. Ekström, S. Ingelman, G. Wannberg, and M. Skarestad, Nucl. Phys. **A311**, 269 (1978).

[22] M.A.J. Mariscotti, G. García Bermúdez, J.C. Acquadro, A. Lepine, M.N. Rao, W. Seale, E. der Mateosian, and P. Thieberger, Phys. Rev. C **19**, 1301 (1979).

[23] G.C. Hicks, C.J. Gross, U.J. Hüttmeier, Xi-Ting Lu, G. Neuschaefer, and S.L. Tabor, Phys. Rev. C **30**, 549 (1984).

[24] J.H. McNeill, Y.A. Akovali, C.R. Bingham, J. Breitenbach, H.K. Carter, J.D. Garrett, J. Kormicki, and P.F. Mantica, Oak Ridge National Laboratory Progress report (1990), p. 63.

[25] J.H. McNeill, A.A. Chishti, W. Gelletly, B.J. Varley, H.G. Price, C.J. Lister, Ö. Skeppstedt, U. Lenz, C.J. Gross, J. Heese, and K.P. Lieb, Manchester University Progress report 1987-1988 (1989), p. 20.

[26] C.J. Lister, B.J. Varley, H.G. Price, and J.W. Olness, Phys. Rev. Lett. **49**, 308 (1982).

[27] S.L. Tabor, M.A. Riley, J. Döring, P.D. Cottle, R. Books, T. Glasmacher, J.W. Holcomb, J. Hutchins, G.D. Johns, T.D. Johnson, T. Petters, O. Tekyi-Mensah, P.C. Womble, L. Wright, and J.X. Saladin, Nucl. Instrum. Methods B **79**, 821 (1993).

[28] S.L. Tabor, Nucl. Instrum. Methods A **265**, 495 (1988).

[29] E.F. Moore, P.D. Cottle, C.J. Gross, D.M. Headly, U.J. Hütt-

meier, S.L. Tabor, and W. Nazarewicz, Phys. Rev. C **38**, 696 (1988).
[30] R.L. Robinson, H.J. Kim, R.O. Sayer, W.T. Milner, R.B. Piercey, J.H. Hamilton, A.V. Ramayya, J.C. Wells, Jr., and A.J. Caffrey, Phys. Rev. C **21**, 603 (1980).
[31] P. Taras and B. Haas, Nucl. Instrum. Methods **123**, 73 (1975).
[32] S. Raman and N.B. Gove, Phys. Rev. C **7**, 1995 (1973).
[33] H. Grawe, P. Hoff, J.P. Omtvedt, K. Steffensen, R. Eder, H. Haas, H. Ravn, and the ISOLDE Collaboration, Z. Phys. A **341**, 247 (1992).
[34] C.F. Liang, P. Paris, D. Bucurescu, S. Della Negra, J. Obert, and J.C. Putaux, Z. Phys. A **309**, 185 (1982).
[35] C.M. Lederer and V.S. Shirley, *Table of Isotopes*, 7th ed. (Wiley, New York, 1978).
[36] E. Nolte and P. Vogt, Z. Phys. A **275**, 33 (1975).
[37] J.F. Ziegler, J.P. Biersack, and U. Littmark, *The Stopping and Range of Ions in Solids* (Pergamon, New York, 1985).
[38] J. Döring, G.D. Johns, R.A. Kaye, M.A. Riley, S.L. Tabor, P.C. Womble, and J.X. Saladin, Phys. Rev. C **52**, R2284 (1995).
[39] B. Cederwall, F. Lidén, A. Johnson, L. Hildingsson, R. Wyss, B. Fant, S. Juutinen, P. Ahonen, S. Mitarai, J. Mukai, J. Nyberg, I. Ragnarsson, and P.B. Semmes, Nucl. Phys. **A542**, 454 (1992).
[40] S.L. Tabor, *Odd Nuclei in the ''Wild West,''* 1st Latin-American Workshop on On and Off Beam Gamma Spectroscopy, Caracas, Venezuela, 1995 (unpublished).
[41] R. Bengtsson, S. Frauendorf, and F.-R. May, At. Data Nucl. Data Tables **35**, 15 (1986).
[42] W. Nazarewicz, J. Dudek, R. Bengtsson, T. Bengtsson, and I. Ragnarsson, Nucl. Phys. **A435**, 397 (1985).
[43] R. Wyss, F. Lidén, J. Nyberg, A. Johnson, D.J.G. Love, A.H. Nelson, D.W. Banes, J. Simpson, A. Kirwan, and R. Bengtsson, Nucl. Phys. **A503**, 244 (1989).
[44] I. Hamamoto and B.R. Mottelson, Phys. Lett. **132B**, 7 (1983).
[45] P. Ring, A. Hayashi, K. Hara, H. Emling, and E. Grosse, Phys. Lett. **110B**, 423 (1982).
[46] W. Nazarewicz, M.A. Riley, and J.D. Garrett, Nucl. Phys. **A512**, 61 (1990).
[47] J. Dudek, W. Nazarewicz, and P. Olanders, Nucl. Phys. **A420**, 285 (1984).